Transcriptional profiling of Hutchinson-Gilford Progeria syndrome fibroblasts reveals deficits in mesenchymal stem cell commitment to differentiation related to early events in endochondral ossification.

Rebeca San Martin [1], Priyojit Das[2], Jacob T. Sanders[1,3], Ashtyn Hill[1], Rachel Patton McCord[1*]

[1] Department of Biochemistry & Cellular and Molecular Biology, University of Tennessee, 309 Ken and Blaire Mossman Bldg. 1311 Cumberland Ave, Knoxville, TN, 37996, USA

[2]UT-ORNL Graduate School of Genome Science and Technology, University of Tennessee, 309 Ken and Blaire Mossman Bldg. 1311 Cumberland Ave, Knoxville, TN, 37996, USA

[3]Department of Pathology, University of Texas Southwestern Medical Center, 5323 Harry Hines Blvd, Dallas TX 75390, USA

*Corresponding author: rmccord@utk.edu ; (865)-974-3149

Abstract

Hutchinson-Gilford Progeria Syndrome results from a mutation in Lamin A, and it is characterized by the incorporation of progerin into the nuclear lamina. Progerin expression leads to alterations in genome architecture, nuclear morphology, and epigenetic states, which in turn cause altered phenotypes in all cells of the mesenchymal lineage. Here, we report a comprehensive analysis of the transcriptional status of patient derived HGPS fibroblasts, including nine cell lines not previously reported. We observe that these fibroblasts carry abnormal transcriptional signatures, centering around five main functional hubs: DNA maintenance and epigenetics, bone development and homeostasis, blood vessel maturation and development, fat deposition and lipid management, and processes related to muscle growth. Stratification of patients by age revealed that a cohort of genes related to endochondral ossification and chondrogenic commitment show altered expression patterns in children aged four to seven years old, where this differentiation program starts in earnest, related to the growth of long bones. We further report changes in lamin associated domains and 3D genome organization around a cohort of genes of interest, identified in this study.

Introduction

Hutchinson-Gilford progeria syndrome (HPGS) is a rare disease, characterized by a severe premature aging phenotype (Gilford, 1897; Hutchinson, 1886). Patients appear normal at birth, with a disease onset around 2 years of age when they present with slow growth rate, short stature, and marked lipodystrophy with a characteristic loss of subcutaneous fat. With progression, patients experience arthritis, joint contracture, osteoporosis and stiffening of blood vessels. Average life expectancy for HPGS patients is 13.4 years, with myocardial infarction and stroke being the predominant causes of death. (Foundation, 2019).

HGPS is caused by a thymidine substitution mutation at cytidine 608 (GGC>GGT), within exon 11 of the gene that encodes for Lamin A (LMNA) (De Sandre-Giovannoli et al., 2003; Eriksson et al., 2003). Lamin A is a structural protein of the nuclear envelope, playing an important role in genome structure and nuclear integrity. The mutation does not result in an amino acid substitution, frame shift or early termination. Rather, it induces the usage of a cryptic splice site and the subsequent deletion of 50 amino acids at the C terminus. In turn, this deletion

impedes downstream processing of the protein and results in conservation of C terminus farnesylation (Davies et al., 2009). This abnormal protein product is called Progerin. Aggregation of Progerin leads to a disruption of the normal nuclear envelope meshwork, leading to deformed nuclei, nuclear stiffening, and defective mechanotransduction (Apte et al., 2017; Goldman et al., 2004; Lammerding et al., 2004).

Of particular interest, progeria patients present with various defects in all tissues of the mesenchymal lineage. Specifically, regarding bone physiology, patients show reduced stature, generalized osteopenia, thin calvaria, and clavicle regression with absence of medial and lateral ends, as well as resorption of the distal bony phalanges and anterior ribs (Chawla et al., 2017; Cleveland et al., 2012; Gordon et al., 2011; Nazir et al., 2017). These phenotypes are more striking when considering that at birth, bone structure appears normal. Previous observations, where fibroblasts from progeria patients showed abnormal levels of aggrecan (Lemire et al., 2006) a marker of chondrogenic differentiation, led us to hypothesize that fibroblasts derived from HGPS patients - themselves a cell of the mesenchymal lineage – could harbor vestigial transcriptional signatures to abnormal mesenchymal stem cell commitment, which would become apparent by comparing them with different normal age group controls.

In this study, we conduct a comprehensive analysis of previously published RNA-seq datasets for HPGS fibroblast lines harboring the typical C>T mutation in the LMNA gene and provide transcriptomics data for nine previously unreported cell lines. By comparing the transcriptional profile of HPGS fibroblasts with cells derived from age matched controls, healthy adults, and healthy old adults, we provide insight into important defects in repair biology, metabolism (calcium, lipid), and other areas of mesenchymal cell lineage import. Our results show that transcription of genes involved in negative regulation of chondrocyte commitment is compromised at an early age, that temporally correlates with the onset of postnatal endochondral ossification, and onset of symptoms. We report that genes central to differentiation commitment into the chondrogenic-osteogenic lineage identified in this study (PTHLP, RUNX2, BMP4 and WNT5a) show either abnormal genomic architecture or lamin associated domain alterations.

Our results support the hypothesis that defects in the initial steps of chondrogenesis commitment are a potential mechanism for mesenchymal stem cell depletion that later results in abnormal adipogenesis, diminished microvasculature homeostasis, and poor wound repair observed in HGPS patients.

Results

Batch correction is essential for comparison among patient and normal cohorts

To determine gene sets that were consistently misregulated in Progeria fibroblasts, we collected both newly generated and previously published RNA-seq data from all available Progeria patient fibroblast cell samples as well as fibroblasts from control individuals in different age groups (Supplementary Tables 1-3) (Fleischer et al., 2018; Ikegami et al., 2020; Köhler et al., 2020; Mateos et al., 2018). When the resulting transcriptomics data were analyzed by principal component analysis (PCA), datasets clustered according to laboratory of origin regardless of diagnosis, making direct comparisons impossible (Supplementary Figure 1A), as has been previously observed in Progeria transcriptomics analysis (Ikegami et al., 2020) However, after batch effect correction (materials and methods (Zhang et al., 2020)), the first principal component was able to segregate the samples depending on progeria/non progeria origin (Supplementary Figure 1B) which enabled direct comparisons between patients and controls from different age groups which originated from different sources.

Gene ontology analysis of transcriptional changes reveals eight clusters of biological activity affected in HGPS

To derive sets of genes differentially regulated in Progeria, we divided the patient samples into Young (0-8 years old) and Teen (>13 years old) categories based on the idea that different developmental processes take place in these age groups. We then compared each patient group to age matched controls, middle aged adults, and older adults and selected up and down-regulated genes (FDR adjusted p-value < 0.001) for gene ontology analysis. Teenage HGPS patients showed the smallest number of genes changing expression levels when compared to age-matched controls, but the highest number of genes up/down regulated when compared to healthy middle aged or old adults (Table 1). Importantly, comparisons between the normal children cohort and the adult normal controls yield few significant changes, suggesting that HGPS is the driver of the differences observed among cohorts.

The largest number of differentially expressed genes (Nine hundred and seventy) were related to the biological processes of epigenetic programming and DNA maintenance (Fig 1-A). Gene ontology pathways included in this cohort include epigenetic regulation of gene silencing, senescence-associated heterochromatin, DNA repair, DNA recombination, and histone methylation/modifications. This is in line with extensive previous evidence of epigenetic and DNA repair misregulation in Progeria (Aguado et al., 2019; Gonzalo and Coll-Bonfill, 2019; Misteli and Scaffidi, 2005)These genes were predominantly over-expressed in young progeria patients when compared to all controls (Fig 1-B, 1-C) and between teenaged patients compared to their age matched control and adults (Fig 1-B, 1-D).

The next biological process with the most misregulated transcription among age groups was tissue repair. It bears mentioning that most of the nucleosome associated proteins and histones identified in the DNA maintenance cluster, as previously described, overlap with the repair GO terms. In all, 585 genes are differentially expressed between cohorts (Fig 2-A), with HGPS patients predominantly over expressing targets pertaining to the organization of the extracellular matrix (145 genes, Fig 2-B). Interestingly, signatures related to coagulation, Bone Morphogenic Protein signaling, and response to wound healing are all downregulated in young HGPS patients when compared to adults (Fig 2-C).

With regards to biology of mesenchymal tissue, mis-regulation of transcription was observed in bone (165 genes. Fig 3), fat (261 genes. Fig 4), blood vessel homeostasis (131 genes. Fig 5), and muscle (261 genes. Fig 6). All of these lineages have been observed as compromised in HGPS patients, showing phenotypes like osteopenia, early atherosclerosis, and lack of subcutaneous fat deposition. (Gordon et al., 2011; Hamczyk et al., 2018; Xiong et al., 2013)

Bone biology mis-regulation appears to be stratified into two distinct hubs: downregulation of pathways related to calcium homeostasis and transport and upregulation of pathways involved in cell differentiation of chondrocytes and osteoblasts (Fig 3-A,3-B). Comparing young patients' transcriptional profile to that of old adult normal controls shows upregulation of genes involved in late osteogenic commitment. Such is the case of ontology terms that include osteoblast differentiation, ossification, and chondrocyte differentiation (Fig3-C). In parallel, genes included in pathways related to cation homeostasis, particularly calcium, are downregulated (Fig 3-D). This comparison is similar to that of young patients and normal middle-aged adult controls (Fig 3-E).

Lipid homeostasis and transport pathways are downregulated in all comparisons between samples from young patients. Young HGPS samples show downregulation in pathways involving fat cell differentiation when compared to age-matched controls, in line with observed fat deposition defects in patients (Revechon et al., 2017) (Fig 4 A-C)

Gene ontology terms related to blood vessels show upregulation of blood vessel morphogenesis, but a decrease of blood vessel maturation when comparing samples from young patients to either age-matched or old controls (Fig 5 A-C). This phenotype persists in comparisons between teen aged patients and their age-matched controls (Fig 5D). Further, in a possible contribution to the circulatory defects observed in HGPS patients, both young and teen-aged patient samples show a marked upregulation of genes in pathways related to muscle development and cardiac muscle differentiation and development when comparing both HGPS cohorts against adult controls (Fig 6 A-C).

To further refine our findings related to young age patients and the mesenchymal phenotypes observed, we stratified the young HGPS patients into two age groups: early infancy (0-3 years old) and children (4-7 years old), comparing these cohorts to age matched, middle age and old controls as before. The total numbers of genes up and down regulated between comparisons are described in Table 2.

About forty percent of genes upregulated in early infant patients when compared against their age matched controls are related to epigenetic modifications as described in the previous analysis (Fig 1). Specifically, the GO term “HDACs deacetylate histones” shows the highest enrichment in this group. These same genes are represented in the comparison with the middle age-old adult control groups.

In contrast, the comparison of patients aged 4-7 y/o to their age matched controls show an enrichment for ossification and calcium homeostasis. Out of the cohort of genes identified as downregulated in this comparison (102), about ten percent are related to early chondrogenesis events. Among those, parathyroid hormone related protein (PTHLH), insulin like growth factor (IGF1), bone morphogenic protein receptor 1B (BMPR1B) and collagen 10a1 (COL10a1), are an integral part of early commitment and control necessary for the triggering of endochondral ossification (Bradley and Drissi, 2010; Green et al., 2015; Maruyama et al., 2010). Genes related to ossification and calcium homeostasis were also identified as downregulated in this cohort. Further, upregulated genes in age-matched and adult comparisons include BMP4, WNT5a, and several genes related to WNT5a biology which play an important role in skeletal development (Fig 7A-B).

Genes of interest are impacted by chromatin compartment switches or abnormal lamina associated domains (LADs)

Chromosome conformation capture was performed on skin fibroblasts of parents of HGPS patients (Mother AG03257, Father HGADFN168) and two HGPS fibroblast cell lines (HGADFN167 and AG11513) (Supplementary Table 4). Genome-wide contact maps for all of these cells show globally similar patterns of chromosome conformation, with the exception of a translocation between chr3 and chr11 in AG11513 cells (Figure 8A). At a whole chromosome folding level, we note that progeria fibroblasts show a decrease in telomere interactions and an apparent loss of ‘Rabl’ like structure (Figure 8B). This type of Rabl structure loss was previously observed after DNA damage in fibroblasts (Sanders et al., 2020). We find that topologically associating domain (TAD) structure is preserved in Progeria fibroblasts, with even an increase in TAD boundary strength as compared to healthy parent controls (Figure 8C). This pattern was also previously observed in DNA damaged fibroblasts, suggesting that some of these features of genome structure may relate to the increased constitutive levels of DNA damage observed in these patient fibroblasts.

Using principal component analysis of Hi-C data at 250 kb-resolution, we classified genomic regions into open euchromatin (A) or closed heterochromatin (B) spatial compartments according to positive and negative values of the first eigenvector, respectively. Since accelerated senescence has been previously observed in progeria fibroblast lines (Bridger and Kill, 2004; Wheaton et al., 2017), we performed compartment analysis on cells

belonging to a matched father-child pair, both at an early and late passages. Samples were collected for the HGADFN168 cells (Father) at passages 12 and 27, and for the HGADFN167 (Child) at passages 12 and 19. Our results show that in the parent cell line there are small changes in compartment strength (the degree of preference for interactions within the same compartment vs. between different compartments). In contrast, there is a predominant loss of A compartment strength in the late passage HGPS cells (Figure 8E). Interestingly, although the compartmentalization strength appears to be altered, the genome-wide compartment identity remains consistent among cohorts, with small changes in compartment identity appearing sporadically (Figure 8D). The loss of compartment strength at later passages in Progeria cells is consistent with previous observations, though this more deeply sequenced, and less noisy dataset shows that compartments are more preserved in Progeria cells than previously observed (McCord et al., 2013).

To test whether the up or downregulation of genes identified through this study relates to compartment switching, we evaluated the compartment identity of all up or downregulated genes, based on their genomic coordinates, in the healthy and patient datasets. While differences between groups are modest, a subset of the genes that are downregulated in the 0-7 HGPS/normal age- matched comparison shift toward the B compartment. This type of trend is also present when comparing HGPS samples from the 0-7 cohort to middle-aged adults but disappears when comparing them to old controls (Figure 8F-H).

To test whether the up or downregulation of genes identified through this study relates to abnormal distribution of lamin associated domains, we compiled the genomic coordinates of these genes with published Lamin ChIP-seq and DamID-seq data (Dekker et al., 2017; McCord et al., 2013). We observe that differences between all groups are significant, with HGPS intensity values markedly higher than their control counterparts (Supplementary Figure 2A and B, Kruskal-Wallis $p<0.001$). However, we found that this shift in Lamin association is true throughout all genomic regions, in an overall dampening of the lamin association signal in HGPS patients (Supplementary Figure 2C), with small regions switching from associated to dissociated from the nuclear lamina. Comparing normal fibroblast cell lines HGADFN168 (belonging to a father of an HGPS patient) and HFFc6 (human foreskin fibroblast), we observe that both show a characteristic bimodal distribution in LAD intensity around markedly positive (LAD) and negative (non-LAD) values (log2 Lamin/input). Remarkably, in contrast, LAD values for the HGPS cell line HGADFN168 distribute normally, around a value of zero: the intensity of both types of association is reduced in HGPS cells, consistent with an overall misregulated interaction between chromosomes and the nuclear lamina (Supplementary Figure 2D).

Downregulated genes of interest related to osteogenesis and chondrogenic proliferation in the early childhood cohorts, as identified by transcriptomics, show alterations in compartment identity or lamina association, but interestingly these changes are not necessarily all the same. For example, the WNT5a gene is located exactly at the boundary between an A/B compartment in both HGPS samples, and in a well-defined A compartment in both parental cell lines. (Fig 9). Importantly, the HGPS in this comparison are from patients in the older childhood cohort, where the marked increase in WNT5a expression that occurs in the younger cohorts disappears. In a contrasting phenotype, the gene that encodes for parathyroid hormone-like hormone (PTHLH) is in a conserved A compartment in both parental and HGPS cell lines (Supplementary Figure 3).

Discussion

In this study we present a comprehensive analysis of the transcriptome of HPGS patient derived fibroblasts, stratified by age, compared to their age-matched controls. Since progeria patients present with accelerated aging, we also compared this data to that derived from middle-aged and old adults. Strikingly, HPGS expression profiles do not phenocopy gene ontology analysis from either set of adult controls, suggesting an altered aging paradigm.

Given the critical role that Lamin A plays in nuclear structure, formation of heterochromatin, and subsequent gene silencing (Lammerding et al., 2004; Leemans et al., 2019), it is not surprising that one of the main biological processes affected in our study, as per gene ontology analysis, is DNA maintenance and epigenetics. Upregulation of genes in the HDAC family is the largest discriminator between Progeria and age-matched normal controls in the 0–3-year-old cohort and 4–7-year-old age groups, and this upregulation persists in comparisons with the adult controls. Our data suggests an upregulation of genes belonging to ontology terms such as negative epigenetic regulation of genes, chromatin silencing, DNA repair, double strand DNA repair and DNA recombination across all age comparison with young patients. Overexpression of these genes are a potential overcompensation mechanism for defects found in DNA repair (Aguado et al., 2019; Gonzalo and Kreienkamp, 2015; Komari et al., 2020; Reviewed by Misteli and Scaffidi, 2005). In older HGPS samples, downregulation of genes related to histone methylation, histone modification, chromatin modifying enzymes, and DNA recombination was also observed.

Concomitant with changes in gene expression of epigenetic factors, Progeria fibroblasts show alterations in chromosome structure, as has been previously observed (McCord et al., 2013). The increased resolution and clarity of Hi-C data presented here enables us to describe these alterations more clearly. Spatial compartmentalization is weakened in Progeria patients with increasing passages consistent with microscopically observed loss of heterochromatin (Goldman et al., 2004). Unlike compartments, topologically associating domain (TAD) boundaries are preserved during in Progeria cells, even at higher passages. When we compare gene expression changes to chromosome structure changes, we observe that many genes consistently upregulated across Progeria patients are in the open, A compartment across all Hi-C samples, suggesting that these gene expression alterations are not associated with dramatic structural change. Downregulated genes are more likely to exhibit switching into the B compartment in Progeria patients.

A compromised transcriptional landscape, related to developmental milestones, points towards a compromised mesenchymal stem cell niche

We further describe up and down regulated biological function clusters that could play a detrimental role in bone, fat, joint and vascular homeostasis. It has been proposed that progerin accumulation in the nucleus results in a defect in the mesenchymal stem cell lineage which gives rise to osteoblasts, chondrocytes, adipocytes, pericytes and myocytes (Reviewed by Andrzejewska et al., 2019). Overall, our results are in concordance with previous reports of transcriptional mis regulation in mesenchymal lineages (Csoka et al., 2004), but the age group comparisons we present here further refine these observations to a temporal effect on lineage commitment.

iPSC models in which HGPS fibroblasts were reprogrammed to stem cells, and further differentiated into mesenchymal stem cells lineages were characterized by nuclear dysmorphia and increased DNA damage, but resulted in confounding results on differentiation, showing either limited differentiation potential, or no significant changes (Crasto and Di Pasquale, 2018; Xiong et al., 2013; Zhang et al., 2011). Interestingly, the most common finding in HGPS-derived iPSCs further differentiated into other lineages is premature senescence and the presence of progerin and misshapen nuclei (Reviewed by Lo Cicero and Nissan, 2015). In a more direct approach, overexpression of progerin A in umbilical cord derived MSCs and other MSC systems resulted in a reduced capacity of differentiation into chondrogenic, osteogenic and adipogenic capacity *in vitro* (Mateos et al., 2013) and deficient proliferation and migration (Pacheco et al., 2014). Spurred by these collective findings, our age-stratified comparisons seek to answer the question of whether this abnormal cell fate regulation occurs predominantly in a particular lineage.

Failed arrest of chondrocyte hypertrophy as a potential mechanism of MSC depletion in HGPS

Transcriptional upregulation of several members of the WNT5a signaling cascade and downregulation of expression of PTHLH, in early age comparisons described in this study, point to an essential defect in early endochondral ossification control and osteogenesis. Specifically, WNT signaling has been previously implicated as a connection between progeria-like syndromes and a defective deposition of extra cellular matrix, essential in bone development (Andrade et al., 2017; Green et al., 2015; Hernandez et al., 2010). Not unlike the phenotypes observed in HGPS patients, bone defects are also present in murine models for HGPS, with young mice (4-week-old) showing decreased trabecular thickness and number, bone volume and decreased mineral density (Hernandez et al., 2010). Not surprisingly, murine pre-osteoblasts forced to express mouse progerin failed to mineralize and show decreased levels of Runx2 expression and alkaline phosphatase upon osteoblastic induction (Tsukune et al., 2019). Further, Lamin A knockdown inhibits osteoblast proliferation and impairs osteoblast differentiation in an MSC in vitro differentiation model (Rauner et al., 2009).

Unlike other MSC fates, like adipogenesis, which occurs downstream of a positive energy intake all through life, bone formation occurs in a carefully orchestrated manner, at specific timepoints during development and early life. Secondary endochondral ossification that occurs in long bones like the humerus and femur, initiate in early childhood, activate intermittently, and finalize with the fusion of the growth plate during the teenage years (Dimeglio et al., 2005; Xie and Chagin, 2021; Zoetis et al., 2003). This process is tightly regulated by several signaling networks aimed at balancing longitudinal growth of the bone with maintenance of precursor cells, like MSCs and quiescent chondrocytes. The transcriptional repression of PTHLH and upregulation of WNT5a in this niche would result in early depletion of the latter, as cells continue down a pathway of chondrocyte proliferation and hypertrophy unimpeded (Bradley and Drissi, 2010; Olsen et al., 2000; Usami et al., 2016). The deficit in clavicular development in HPGS patients could provide some insight as to the spatiotemporal consequences of MSC/chondrocyte pool depletion. The clavicle is unique because while it is the first bone to start ossification during the embryonic period (Ogata and Uhthoff, 1990), it is the last to complete the process. In early events, around the fifth week of gestation, the two primary ossification centers, formed from mesenchymal tissues, fuse to form the middle of the clavicle. The complete ossification of the clavicular epiphysis occurs via endochondral ossification during the teenage years, with medial ossification beginning at the onset of puberty (Ferguson and Scott, 2015; Langley, 2016). In turn, bone deposition at the terminal ossification center, must occur in adolescents between 11 and 16 years of age, for the process to successfully proceed to epiphyseal plate ossification in early adulthood. (Schulz et al., 2008). Taken together, our observations point towards a “fail to arrest” phenotype that results in over-commitment towards the hypertrophic chondrocyte lineage in very young HGPS patients. We hypothesize that this results in a premature depletion of the chondro-osteoprogenitor pool and, at later stages, of the bone marrow-derived mesenchymal stem cells that feed into this niche with later in life result in the incomplete endochondral ossification of the claviculae of HGPS patients (Movie 1).

Deficient repair responses exacerbate the depletion of tissue resident MSC pools

A secondary function of tissue resident MSCs is to aid in repair during wounding and disease.
Our data shows that dermal fibroblasts derived from HPGS patients present with abnormal repair, including downregulated signatures of wound healing, hemostasis, and BMP signaling. These observations recapitulate previous reports of HGPS patient-derived skin precursors, which can differentiate intro fibroblasts and smooth muscle cells (smooth muscle alpha actin positive – myofibroblasts). In the precursor stage, these cells express low levels of progerin *in vivo* and *in vitro*, but differentiation into the lineages increases progerin expression and deposition in the nucleus (Wenzel et al., 2012). In concordance with our findings, a progeria murine model, deficient in the downstream processing of lamin A, shows abnormal skin wound repair, with prolonged time to wound closure, poor vasculogenic signaling and angiogenesis, which includes a limited mobilization of bone-marrow derived progenitor cells (Butala et al., 2012). Related to this phenotype, the LMNAΔ9 murine progeria model for HPGS show a significant decrease in postnatal fibroblast proliferation, with accelerated senescence

levels in cell lines derived from kidney, lung, skin, and skeletal muscle (Hernandez et al., 2010). Further, a decreased epidermal population of adult stem cells was observed in another murine model of HGPS (Rosengardten et al., 2011), which are also deficient for skin wound repair.

Overall, growth, development, and maintaining homeostasis place a considerable burden on the mesenchymal stem cell pool and its many lineages. Under a paradigm of biology of priority during development the organism's structural integrity in the shape of bones and joints, the homeostasis of blood microvessels – regulated by pericytes - should take precedence to fat deposition (Figure 10A).

We propose that these defects in repair in Progeria patients strain the mesenchymal stem cell pools from which repair reactive stroma originates, which have been characterized as both pools of CD44/CD99 positive cells in glandular tissues and as pluripotent cells located at the pericyte position (Crisan et al., 2008; Kim et al., 2014). Interestingly, it has been reported that normal fibroblast cell lines contain a subset of pluripotent MSCs, indistinguishable from those derived from the bone marrow (Denu et al., 2016) and it is established that normal MSCs lose proliferative and differentiation potential within a few passages when cultured *in vitro*. This phenomenon has been correlated with a defect in lamin A maturation that leads to cellular senescence (Bellotti et al., 2016), which is similar to the terminal differentiation into wound-repair-myofibroblasts resulting from the TGF-beta induction of prostate resident MSCs (Kim et al., 2014). HPGS fibroblasts experience an increased rate in apoptosis, with subsequent cell divisions, concomitant with mutant Lamin A accumulation (Bridger and Kill, 2004), and chronic DNA damage that lead to premature senescence (Wheaton et al., 2017),which could be indirect evidence of early depletion of the MSC pool in these cell lines. (Figure 10B).

Related to later differentiation events, the depletion of microvasculature resident MSCs occurring as a result of chronic, deficient wound repair will carry a severe impact to adipogenesis. Cells at the pericyte position have been characterized as the primary source for adipocytes *in vivo* (Traktuev et al., 2008; Zannettino et al., 2008). These cells, which are CD44, CD90 double positive, phenocopy the pluripotency of tissue resident mesenchymal stem cells, and are able to differentiate into repair-like myofibroblasts expressing smooth muscle alpha actin (Merfeld-Clauss et al., 2017). Coupled with a preadipocyte depletion phenotype, lipodystrophy in HGPS has also been experimentally induced by the introduction of progerin expression into a subset of pre adipogenic cells in mice, which led to fibrosis, senescence, and macrophage infiltration, with the ultimate result of white fat depletion (Revechon et al., 2017).

The fibroblast as a sentinel of general mesenchymal lineage health

The criticism can be made that it is a stretch to make hypotheses about different mesenchymal stem cell pools based only on gene expression from dermal fibroblasts. However, mounting evidence has shown that after birth, the bone marrow mesenchymal stem cell niche is in close synergy with pools of fibroblasts (LeBleu and Neilson, 2020; Soundararajan and Kannan, 2018), tissue resident mesenchymal stem cells (El Agha et al., 2017) and pericytes (Lamagna and Bergers, 2006). Since these cell pools are in flux, and can compensate for each other under duress (Di Carlo and Peduto, 2018; Direkze et al., 2004; Ozerdem et al., 2005; San Martin et al., 2014), comparing the global transcriptional status of fibroblasts between a patient cohort and its aged-matched controls can provide an insight into potential systemic deficits and compensatory mechanisms at play.

Ideas and speculation

Overall, the cohorts of biological processes that we observe to be misregulated across different age groups of Progeria patients lead us to speculate the impact of this misregulation across a series of events in development, which will warrant further investigation:

A. Biology of priority: the formation of bone "fires" at specific times, these events are "non-negotiable" and will take precedence over any other concomitant MSC fates. Deficits in endochondral ossification will draw from pericyte and tissue resident MSCs in an attempt to compensate.
B. The loss of bone fusion and regression of bone length observed in teenaged HGPS patients is an indirect result of deficits in arrest of chondrogenesis proliferation, that occurred in early childhood. These deficits resulted in depletion of MSC pools, both in the bone marrow and in tissues
C. Depletion of the pericyte niche is exacerbated by a chronic, incompetent, wound repair response. Ultimately, this depletion will result in loss of microvasculature integrity and subsequent vascular events observed in HGPS, such as vascular stiffness and atherosclerosis.
D. Elaborating on proposed MSC interventions (Infante and Rodriguez, 2021) and current gene editing efforts (Koblan et al., 2021), targeting the bone marrow niche in young patients could rescue the later HGPS phenotypes.

Materials and Methods

RNA-seq

Ten micrograms of purified RNA from several progeria cell lines were acquired from the Coriell Institute (Camden, NJ) as follows: AG06917 (HGPS. Male 3 y/o), AG10578 (HGPS. Male 17 y/o), AG11572 (HGPS. Female 2 y/o), AG10677 (HGPS. Male 4 y/o), AG08466 (HGPS. Female 8 y/o), AG03198 (HGPS. Female 10 y/o), AG07493 (HGPS. Female 2 y/o), AG01178 (HGPS. Male 20 y/o), AG11513 (HGPS. Female 8 y/o, GM01972 (HGPS. Female 14 y/o), GM01178 (HGPS. Male 20 y/o). After internal quality control upon receipt, RNA-seq library construction and sequencing was carried out by Genewiz (South Plainfield, NJ). Further, previously published RNA-seq datasets from HPGS cell lines and normal controls were included in the study (Supplementary Tables 1-3) (Fleischer et al., 2018; Ikegami et al., 2020; Köhler et al., 2020; Mateos et al., 2018).

RNA-seq data processing

The fastq reads were first processed with BBDuk tool (https://github.com/kbaseapps/BBTools), performing adapter trimming with parameters "ktrim=r k=23 mink=11 hdist=1". Adapter trimmed reads were processed for quality trimming using the BBDuk tool to discard reads with quality score lower than 28 (parameters "qtrim=r trimq=28"). Following the adapter and quality trimming steps, the reads were aligned to the reference genome hg19 using STAR aligner (https://github.com/alexdobin/STAR) with both '--outFilterScoreMinOverLread' and ' –outFilterMatchNminOverLread' parameters set to 0.2. Finally, the mapped reads were sorted based on genomic coordinates and feature count was performed with HTSeq-Counts (https://github.com/simon-anders/htseq).

Batch effect removal

Since the RNA-seq files used in this study were generated in different laboratories, using different technologies, the raw gene counts produced by HTSeq-Counts suffer from batch effect. To mitigate that issue, the raw counts are batch effect adjusted using the ComBat-seq tool (https://github.com/zhangyuqing/ComBat-seq). For this purpose, files from the same laboratory are assigned the same batch number. In addition, the sex and status of the samples are provided as the biological covariates to the ComBat-seq tool to preserve that signal in the adjusted data.

Differential expression analysis

Differential gene expression analysis was performed between different groups of diseased and healthy samples using DESeq2 (https://bioconductor.org/packages/release/bioc/html/DESeq2.html) tool. HGPS samples from Young (0-7 y/o) or teenage (13+ y/o) patients were compared to age matched (AM), middle aged (M), and old (O) control samples (Supplementary Data). Further, to correlate gene expression profiles with known patient

survival statistics, comparisons were further refined by stratifying early infancy progeria patients (0-3 years old) and older children (4-7 years old), comparing those populations to age matched, middle aged and old control samples, as before.

Gene ontology analysis

Genes defined as up/down regulated for each of the age group comparisons, were considered for gene ontology analysis based on a p adjusted value cutoff of 0.001. These gene lists, in turn, were then analyzed using Metascape (Zhou et al., 2019). Metascape output files were manually clustered into gene ontology themes, observed throughout the analysis. Gene lists derived from this manual clustering were then visualized via heatmaps to facilitate comparisons among age groups.

Gene expression heatmap plotting

To plot expression of specific genes across different samples as a heatmap, the batch adjusted counts for all the genes for each sample were log2 normalized with a pseudo count of 1. The expression of specific genes across specific samples was then extracted and Z-score normalization was performed for each of the genes. Finally, the Z-score normalized values were plotted using the Seaborn python package as a heatmap. (https://seaborn.pydata.org/)

DamID-seq data processing

All the DamID-seq data was processed as previously reported (Leemans et al., 2019), with modifications in the trimming step. Briefly, the bwa mem (https://github.com/lh3/bwa) tool was used to map gDNA reads starting with GATC to a combination of hg19 reference genome with a ribosomal model. For further processing, only the mapped reads having a mapping quality of at least 10 were considered as GATC fragments. Next, the reads were combined into the bins of 40 kb resolution depending on the middle of the GATC fragments and then scaled to 1M reads. For normalization, log2-ratio of the scaled target over the scaled Dam-only bins was calculated with a pseudo count of 1.

Cell culture

Human primary dermal fibroblast cell lines were obtained from The Progeria Research Foundation (PRF) Cell and Tissue Bank. The HGPS cell lines were HGADFN167 and HGADFN168. Normal dermal fibroblasts AG11513 and AG03257 were purchased from Coriell Institute (Camden, NJ). Cells were grown in DMEM (Gibco) supplemented with 15% FBS (Corning), 1% Pen-strep (Gibco), and 1% L-glutamine (Gibco). Cells were passaged at a density of 80%.

Chromosome conformation capture (Hi-C)

Hi-C experiments were performed according to standard protocols (Golloshi et al., 2018). The starting material was comprised of skin fibroblasts of parents of HGPS patients (Mother AG03257, Father HGADFN168) and two HGPS fibroblast cell lines (HGADFN167 and AG11513). Further, HGADFN168 and HGADFN167, belonging to a parent-child matched cells were analyzed both at an early and late passage: p12-27 and p12-19, respectively.

Briefly, ~5 million cells were fixed with 1% formaldehyde, suspended in cell lysis buffer for permeabilization, and homogenized by douncing. Crosslinked chromatin was digested overnight with HindIII (HGADFN167 and HGADFN168) or DpnII (HGADFN167, HGADFN168, AG03257 and AG11513). Sticky ends were filled in with biotin-dATP (Invitrogen), and the blunt ends of interacting fragments were ligated together. DNA was purified by two phenol-chloroform extractions and ethanol precipitation. Biotin-dATP at unligated ends was removed, and the DNA was sheared to a target size of 200-400 bp by a Covaris sonicator (Covaris, M220). DNA between 100-400 bp was selected for using AMPure XP beads (Beckman Coulter). Biotinylated DNA was pulled down using streptavidin coated magnetic beads and prepared for multiplex sequencing on an Illumina platform using the

NEBNext Ultra II kit (NEB, E7645S). All end preparation, adaptor ligation, and PCR amplification steps were carried out on bead bound DNA libraries. Sequencing was carried out on Illumina HiSeq 3000 or NovaSeq platforms with 75 bp or 150 bp paired end reads. All Hi-C data statistics are presented in Supplementary Table 4.

Analysis of Hi-C data

Sequencing reads were mapped to the reference human genome hg19, filtered, and iteratively corrected using previously published pipelines (Imakaev et al., 2012), available on github (https://github.com/dekkerlab/cMapping). Publicly available tools (https://github.com/dekkerlab/cworld-dekker) were used to produce Hi-C heatmaps at 2.5 Mb and 250 kb resolution and to perform principal component analysis (using the matrix2compartment script) to generate compartment tracks at 250 kb resolution, assigning A and B compartments to positive and negative PC1 values, respectively. Values from replicate experiments were averaged, by bin, to produce the final compartment track. TAD boundary strength analysis was carried out using the insulation score approach (Crane et al., 2015) (matrix2insulation) from this cworld package with 500 kb insulation square using 40 kb resolution contact maps.

ChIP-seq data and processing: Lamin Associated Domain Analysis

Raw LMNA ChIP-seq data was obtained from the NCBI Gene Expression Omnibus (GEO) (http://www.ncbi.nlm.nih.gov/geo/) under accession number GSE41764 (McCord et al., 2013). For comparison, DamID-seq for the fibroblast line HFFc6 (van Steensel Lab, Netherlands Cancer Institute) was obtained from the 4D Nucleome data portal (Dekker et al., 2017; Reiff et al., 2021), through the bio sample identifier 4DNBSR7TC87A https://data.4dnucleome.org/biosamples/4DNBSR7TC87A/.
The fastq reads were first processed for adapter and quality trimming with the help of BBDuk tool (https://github.com/kbaseapps/BBTools). The reads were then aligned to the hg19 reference genome using STAR aligner (https://github.com/alexdobin/STAR). Finally, both the target and input mapped reads were binned at 40 kb resolution and log2-ratio of the target over the input bins was calculated using the 'bamCompare' function of deepTools (https://deeptools.readthedocs.io/) with parameters "--operation log2 -bs 40000 --ignoreDuplicates --minMappingQuality 30 --scaleFactorsMethod SES --effectiveGenomeSize 2864785220".

Data availability

All RNA-seq and Hi-C data contributed by this study is available on GEO at GSEXXXX.

Acknowledgements

The authors would like to thank Enrique Pacheco San Martin for his assistance with graphics and media design. The concept of the biology of priority during development and repair was adapted from discussion with, and coursework designed by, David Rowley Ph.D. (Baylor College of Medicine). This work was supported by NIH NIGMS Grant R35GM133557 to R.P.M. R. San Martin was supported by a postdoctoral fellowship from the American Cancer Society (134060-PF-19-183-01-CSM).

Author Contributions

The study was conceived and designed by RSM, JTS, and RPM. Experimental data were collected by JTS and AH. Data analysis was performed by RSM, PD, JTS, and RPM. RSM and RPM wrote the manuscript with input from all authors. The project was supervised by RPM.

Competing Interests

The authors declare no competing financial interests.

References

Aguado, J., Sola-Carvajal, A., Cancila, V., Revechon, G., Ong, P.F., Jones-Weinert, C.W., Wallen Arzt, E., Lattanzi, G., Dreesen, O., Tripodo, C.*, et al.* (2019). Inhibition of DNA damage response at telomeres improves the detrimental phenotypes of Hutchinson-Gilford Progeria Syndrome. Nat Commun *10*, 4990.

Andrade, A.C., Jee, Y.H., and Nilsson, O. (2017). New Genetic Diagnoses of Short Stature Provide Insights into Local Regulation of Childhood Growth. Horm Res Paediatr *88*, 22-37.

Andrzejewska, A., Lukomska, B., and Janowski, M. (2019). Concise Review: Mesenchymal Stem Cells: From Roots to Boost. Stem Cells *37*, 855-864.

Apte, K., Stick, R., and Radmacher, M. (2017). Mechanics in human fibroblasts and progeria: Lamin A mutation E145K results in stiffening of nuclei. J Mol Recognit *30*.

Bellotti, C., Capanni, C., Lattanzi, G., Donati, D., Lucarelli, E., and Duchi, S. (2016). Detection of mesenchymal stem cells senescence by prelamin A accumulation at the nuclear level. Springerplus *5*, 1427.

Bradley, E.W., and Drissi, M.H. (2010). WNT5A regulates chondrocyte differentiation through differential use of the CaN/NFAT and IKK/NF-kappaB pathways. Mol Endocrinol *24*, 1581-1593.

Bridger, J.M., and Kill, I.R. (2004). Aging of Hutchinson-Gilford progeria syndrome fibroblasts is characterised by hyperproliferation and increased apoptosis. Exp Gerontol *39*, 717-724.

Butala, P., Szpalski, C., Soares, M., Davidson, E.H., Knobel, D., and Warren, S.M. (2012). Zmpste24-/- mouse model for senescent wound healing research. Plast Reconstr Surg *130*, 788e-798e.

Chawla, G.S., Agrawal, P.M., and Dhok, A. (2017). Progeria: an extremely unusual disorder. Skeletal Radiol *46*, 1149-1153.

Cleveland, R.H., Gordon, L.B., Kleinman, M.E., Miller, D.T., Gordon, C.M., Snyder, B.D., Nazarian, A., Giobbie-Hurder, A., Neuberg, D., and Kieran, M.W. (2012). A prospective study of radiographic manifestations in Hutchinson-Gilford progeria syndrome. Pediatr Radiol *42*, 1089-1098.

Crane, E., Bian, Q., McCord, R.P., Lajoie, B.R., Wheeler, B.S., Ralston, E.J., Uzawa, S., Dekker, J., and Meyer, B.J. (2015). Condensin-driven remodelling of X chromosome topology during dosage compensation. Nature *523*, 240-244.

Crasto, S., and Di Pasquale, E. (2018). Induced Pluripotent Stem Cells to Study Mechanisms of Laminopathies: Focus on Epigenetics. Front Cell Dev Biol *6*, 172.

Crisan, M., Yap, S., Casteilla, L., Chen, C.W., Corselli, M., Park, T.S., Andriolo, G., Sun, B., Zheng, B., Zhang, L.*, et al.* (2008). A perivascular origin for mesenchymal stem cells in multiple human organs. Cell Stem Cell *3*, 301-313.

Csoka, A.B., English, S.B., Simkevich, C.P., Ginzinger, D.G., Butte, A.J., Schatten, G.P., Rothman, F.G., and Sedivy, J.M. (2004). Genome-scale expression profiling of Hutchinson-Gilford progeria syndrome reveals widespread transcriptional misregulation leading to mesodermal/mesenchymal defects and accelerated atherosclerosis. Aging Cell *3*, 235-243.

Davies, B.S., Fong, L.G., Yang, S.H., Coffinier, C., and Young, S.G. (2009). The posttranslational processing of prelamin A and disease. Annu Rev Genomics Hum Genet *10*, 153-174.

De Sandre-Giovannoli, A., Bernard, R., Cau, P., Navarro, C., Amiel, J., Boccaccio, I., Lyonnet, S., Stewart, C.L., Munnich, A., Le Merrer, M.*, et al.* (2003). Lamin a truncation in Hutchinson-Gilford progeria. Science *300*, 2055.

Dekker, J., Belmont, A.S., Guttman, M., Leshyk, V.O., Lis, J.T., Lomvardas, S., Mirny, L.A., O'Shea, C.C., Park, P.J., Ren, B.*, et al.* (2017). The 4D nucleome project. Nature *549*, 219-226.

Denu, R.A., Nemcek, S., Bloom, D.D., Goodrich, A.D., Kim, J., Mosher, D.F., and Hematti, P. (2016). Fibroblasts and Mesenchymal Stromal/Stem Cells Are Phenotypically Indistinguishable. Acta Haematol *136*, 85-97.

Di Carlo, S.E., and Peduto, L. (2018). The perivascular origin of pathological fibroblasts. J Clin Invest *128*, 54-63.

Dimeglio, A., Charles, Y.P., Daures, J.P., de Rosa, V., and Kabore, B. (2005). Accuracy of the Sauvegrain method in determining skeletal age during puberty. J Bone Joint Surg Am *87*, 1689-1696.

Direkze, N.C., Hodivala-Dilke, K., Jeffery, R., Hunt, T., Poulsom, R., Oukrif, D., Alison, M.R., and Wright, N.A. (2004). Bone marrow contribution to tumor-associated myofibroblasts and fibroblasts. Cancer Res *64*, 8492-8495.

El Agha, E., Kramann, R., Schneider, R.K., Li, X., Seeger, W., Humphreys, B.D., and Bellusci, S. (2017). Mesenchymal Stem Cells in Fibrotic Disease. Cell Stem Cell *21*, 166-177.
Eriksson, M., Brown, W.T., Gordon, L.B., Glynn, M.W., Singer, J., Scott, L., Erdos, M.R., Robbins, C.M., Moses, T.Y., Berglund, P.*, et al.* (2003). Recurrent de novo point mutations in lamin A cause Hutchinson-Gilford progeria syndrome. Nature *423*, 293-298.
Ferguson, D., and Scott, B. (2015). The enigmatic role and development of the clavicle. ORTHOPAEDICS AND TRAUMA *30*.
Fleischer, J.G., Schulte, R., Tsai, H.H., Tyagi, S., Ibarra, A., Shokhirev, M.N., Huang, L., Hetzer, M.W., and Navlakha, S. (2018). Predicting age from the transcriptome of human dermal fibroblasts. Genome biology *19*, 221-221.
Foundation, P.R. (2019). The Progeria Handbook. A guide for Families & Health Care Providers of Children with Progeria, 2nd edn (Peabody, MA: Progeria Research Foundation).
Gilford, H. (1897). On a Condition of Mixed Premature and Immature Development. Med Chir Trans *80*, 17-46 25.
Goldman, R.D., Shumaker, D.K., Erdos, M.R., Eriksson, M., Goldman, A.E., Gordon, L.B., Gruenbaum, Y., Khuon, S., Mendez, M., Varga, R.*, et al.* (2004). Accumulation of mutant lamin A causes progressive changes in nuclear architecture in Hutchinson-Gilford progeria syndrome. Proc Natl Acad Sci U S A *101*, 8963-8968.
Golloshi, R., Sanders, J.T., and McCord, R.P. (2018). Iteratively improving Hi-C experiments one step at a time. Methods *142*, 47-58.
Gonzalo, S., and Coll-Bonfill, N. (2019). Genomic instability and innate immune responses to self-DNA in progeria. Geroscience *41*, 255-266.
Gonzalo, S., and Kreienkamp, R. (2015). DNA repair defects and genome instability in Hutchinson-Gilford Progeria Syndrome. Curr Opin Cell Biol *34*, 75-83.
Gordon, C.M., Gordon, L.B., Snyder, B.D., Nazarian, A., Quinn, N., Huh, S., Giobbie-Hurder, A., Neuberg, D., Cleveland, R., Kleinman, M.*, et al.* (2011). Hutchinson-Gilford progeria is a skeletal dysplasia. J Bone Miner Res *26*, 1670-1679.
Green, J.D., Tollemar, V., Dougherty, M., Yan, Z., Yin, L., Ye, J., Collier, Z., Mohammed, M.K., Haydon, R.C., Luu, H.H.*, et al.* (2015). Multifaceted signaling regulators of chondrogenesis: Implications in cartilage regeneration and tissue engineering. Genes Dis *2*, 307-327.
Hamczyk, M.R., Villa-Bellosta, R., Gonzalo, P., Andres-Manzano, M.J., Nogales, P., Bentzon, J.F., Lopez-Otin, C., and Andres, V. (2018). Vascular Smooth Muscle-Specific Progerin Expression Accelerates Atherosclerosis and Death in a Mouse Model of Hutchinson-Gilford Progeria Syndrome. Circulation *138*, 266-282.
Hernandez, L., Roux, K.J., Wong, E.S., Mounkes, L.C., Mutalif, R., Navasankari, R., Rai, B., Cool, S., Jeong, J.W., Wang, H.*, et al.* (2010). Functional coupling between the extracellular matrix and nuclear lamina by Wnt signaling in progeria. Dev Cell *19*, 413-425.
Hutchinson, J. (1886). Congenital Absence of Hair and Mammary Glands with Atrophic Condition of the Skin and its Appendages, in a Boy whose Mother had been almost wholly Bald from Alopecia Areata from the age of Six. Med Chir Trans *69*, 473-477.
Ikegami, K., Secchia, S., Almakki, O., Lieb, J.D., and Moskowitz, I.P. (2020). Phosphorylated Lamin A/C in the Nuclear Interior Binds Active Enhancers Associated with Abnormal Transcription in Progeria. Dev Cell *52*, 699-713 e611.
Imakaev, M., Fudenberg, G., McCord, R.P., Naumova, N., Goloborodko, A., Lajoie, B.R., Dekker, J., and Mirny, L.A. (2012). Iterative correction of Hi-C data reveals hallmarks of chromosome organization. Nat Methods *9*, 999-1003.
Infante, A., and Rodriguez, C.I. (2021). Cell and Cell-Free Therapies to Counteract Human Premature and Physiological Aging: MSCs Come to Light. J Pers Med *11*.

Kim, W., Barron, D.A., San Martin, R., Chan, K.S., Tran, L.L., Yang, F., Ressler, S.J., and Rowley, D.R. (2014). RUNX1 is essential for mesenchymal stem cell proliferation and myofibroblast differentiation. Proceedings of the National Academy of Sciences of the United States of America *111*, 16389-16394.
Koblan, L.W., Erdos, M.R., Wilson, C., Cabral, W.A., Levy, J.M., Xiong, Z.M., Tavarez, U.L., Davison, L.M., Gete, Y.G., Mao, X.*, et al.* (2021). In vivo base editing rescues Hutchinson-Gilford progeria syndrome in mice. Nature *589*, 608-614.
Köhler, F., Bormann, F., Raddatz, G., Gutekunst, J., Corless, S., Musch, T., Lonsdorf, A.S., Erhardt, S., Lyko, F., and Rodríguez-Paredes, M. (2020). Epigenetic deregulation of lamina-associated domains in Hutchinson-Gilford progeria syndrome. Genome Med *12*, 46-46.
Komari, C.J., Guttman, A.O., Carr, S.R., Trachtenberg, T.L., Orloff, E.A., Haas, A.V., Patrick, A.R., Chowdhary, S., Waldman, B.C., and Waldman, A.S. (2020). Alteration of genetic recombination and double-strand break repair in human cells by progerin expression. DNA Repair (Amst) *96*, 102975.
Lamagna, C., and Bergers, G. (2006). The bone marrow constitutes a reservoir of pericyte progenitors. J Leukoc Biol *80*, 677-681.
Lammerding, J., Schulze, P.C., Takahashi, T., Kozlov, S., Sullivan, T., Kamm, R.D., Stewart, C.L., and Lee, R.T. (2004). Lamin A/C deficiency causes defective nuclear mechanics and mechanotransduction. J Clin Invest *113*, 370-378.
Langley, N.R. (2016). The lateral clavicular epiphysis: fusion timing and age estimation. Int J Legal Med *130*, 511-517.
LeBleu, V.S., and Neilson, E.G. (2020). Origin and functional heterogeneity of fibroblasts. FASEB J *34*, 3519-3536.
Leemans, C., van der Zwalm, M.C.H., Brueckner, L., Comoglio, F., van Schaik, T., Pagie, L., van Arensbergen, J., and van Steensel, B. (2019). Promoter-Intrinsic and Local Chromatin Features Determine Gene Repression in LADs. Cell *177*, 852-864 e814.
Lemire, J.M., Patis, C., Gordon, L.B., Sandy, J.D., Toole, B.P., and Weiss, A.S. (2006). Aggrecan expression is substantially and abnormally upregulated in Hutchinson-Gilford Progeria Syndrome dermal fibroblasts. Mech Ageing Dev *127*, 660-669.
Lo Cicero, A., and Nissan, X. (2015). Pluripotent stem cells to model Hutchinson-Gilford progeria syndrome (HGPS): Current trends and future perspectives for drug discovery. Ageing Res Rev *24*, 343-348.
Maruyama, T., Mirando, A.J., Deng, C.X., and Hsu, W. (2010). The balance of WNT and FGF signaling influences mesenchymal stem cell fate during skeletal development. Sci Signal *3*, ra40.
Mateos, J., De la Fuente, A., Lesende-Rodriguez, I., Fernández-Pernas, P., Arufe, M.C., and Blanco, F.J. (2013). Lamin A deregulation in human mesenchymal stem cells promotes an impairment in their chondrogenic potential and imbalance in their response to oxidative stress. Stem Cell Research *11*, 1137-1148.
Mateos, J., Fafián-Labora, J., Morente-López, M., Lesende-Rodriguez, I., Monserrat, L., Ódena, M.A., Oliveira, E.d., de Toro, J., and Arufe, M.C. (2018). Next-Generation Sequencing and Quantitative Proteomics of Hutchinson-Gilford progeria syndrome-derived cells point to a role of nucleotide metabolism in premature aging. PloS one *13*, e0205878-e0205878.
McCord, R.P., Nazario-Toole, A., Zhang, H., Chines, P.S., Zhan, Y., Erdos, M.R., Collins, F.S., Dekker, J., and Cao, K. (2013). Correlated alterations in genome organization, histone methylation, and DNA-lamin A/C interactions in Hutchinson-Gilford progeria syndrome. Genome Res *23*, 260-269.
Merfeld-Clauss, S., Lease, B.R., Lu, H., March, K.L., and Traktuev, D.O. (2017). Adipose stromal cells differentiation toward smooth muscle cell phenotype diminishes their vasculogenic activity due to induction of activin A secretion. J Tissue Eng Regen Med *11*, 3145-3156.
Misteli, T., and Scaffidi, P. (2005). Genome instability in progeria: when repair gets old. Nat Med *11*, 718-719.
Nazir, H.M., Ramesh Baabhu, A., Muralidharan, Y., and Cheppala Rajan, S. (2017). Radiological Diagnosis of a Rare Premature Aging Genetic Disorder: Progeria (Hutchinson-Gilford Syndrome). Case Rep Radiol *2017*, 1305360.

Ogata, S., and Uhthoff, H.K. (1990). The early development and ossification of the human clavicle--an embryologic study. Acta Orthop Scand *61*, 330-334.
Olsen, B.R., Reginato, A.M., and Wang, W. (2000). Bone development. Annual review of cell and developmental biology *16*, 191-220.
Ozerdem, U., Alitalo, K., Salven, P., and Li, A. (2005). Contribution of bone marrow-derived pericyte precursor cells to corneal vasculogenesis. Invest Ophthalmol Vis Sci *46*, 3502-3506.
Pacheco, L.M., Gomez, L.A., Dias, J., Ziebarth, N.M., Howard, G.A., and Schiller, P.C. (2014). Progerin expression disrupts critical adult stem cell functions involved in tissue repair. Aging (Albany NY) *6*, 1049-1063.
Rauner, M., Sipos, W., Goettsch, C., Wutzl, A., Foisner, R., Pietschmann, P., and Hofbauer, L.C. (2009). Inhibition of lamin A/C attenuates osteoblast differentiation and enhances RANKL-dependent osteoclastogenesis. J Bone Miner Res *24*, 78-86.
Reiff, S.B., Schroeder, A.J., Kirli, K., Cosolo, A., Bakker, C., Mercado, L., Lee, S., Veit, A.D., Balashov, A.K., Vitzthum, C*., et al.* (2021). The 4D Nucleome Data Portal: a resource for searching and visualizing curated nucleomics data. bioRxiv.
Revechon, G., Viceconte, N., McKenna, T., Sola Carvajal, A., Vrtacnik, P., Stenvinkel, P., Lundgren, T., Hultenby, K., Franco, I., and Eriksson, M. (2017). Rare progerin-expressing preadipocytes and adipocytes contribute to tissue depletion over time. Sci Rep *7*, 4405.
Rosengardten, Y., McKenna, T., Grochova, D., and Eriksson, M. (2011). Stem cell depletion in Hutchinson-Gilford progeria syndrome. Aging Cell *10*, 1011-1020.
San Martin, R., Barron, D.A., Tuxhorn, J.A., Ressler, S.J., Hayward, S.W., Shen, X., Laucirica, R., Wheeler, T.M., Gutierrez, C., Ayala, G.E*., et al.* (2014). Recruitment of CD34(+) fibroblasts in tumor-associated reactive stroma: the reactive microvasculature hypothesis. Am J Pathol *184*, 1860-1870.
Sanders, J.T., Freeman, T.F., Xu, Y., Golloshi, R., Stallard, M.A., Hill, A.M., San Martin, R., Balajee, A.S., and McCord, R.P. (2020). Radiation-induced DNA damage and repair effects on 3D genome organization. Nature Communications *11*, 6178.
Schulz, R., Zwiesigk, P., Schiborr, M., Schmidt, S., and Schmeling, A. (2008). Ultrasound studies on the time course of clavicular ossification. Int J Legal Med *122*, 163-167.
Soundararajan, M., and Kannan, S. (2018). Fibroblasts and mesenchymal stem cells: Two sides of the same coin? J Cell Physiol *233*, 9099-9109.
Traktuev, D.O., Merfeld-Clauss, S., Li, J., Kolonin, M., Arap, W., Pasqualini, R., Johnstone, B.H., and March, K.L. (2008). A population of multipotent CD34-positive adipose stromal cells share pericyte and mesenchymal surface markers, reside in a periendothelial location, and stabilize endothelial networks. Circ Res *102*, 77-85.
Tsukune, N., Naito, M., Ohashi, A., Ninomiya, T., Sato, S., and Takahashi, T. (2019). Forced expression of mouse progerin attenuates the osteoblast differentiation interrupting beta-catenin signal pathway in vitro. Cell Tissue Res *375*, 655-664.
Usami, Y., Gunawardena, A.T., Iwamoto, M., and Enomoto-Iwamoto, M. (2016). Wnt signaling in cartilage development and diseases: lessons from animal studies. Lab Invest *96*, 186-196.
Wenzel, V., Roedl, D., Gabriel, D., Gordon, L.B., Herlyn, M., Schneider, R., Ring, J., and Djabali, K. (2012). Naïve adult stem cells from patients with Hutchinson-Gilford progeria syndrome express low levels of progerin in vivo. Biology Open *1*, 516-526.
Wheaton, K., Campuzano, D., Ma, W., Sheinis, M., Ho, B., Brown, G.W., and Benchimol, S. (2017). Progerin-Induced Replication Stress Facilitates Premature Senescence in Hutchinson-Gilford Progeria Syndrome. Mol Cell Biol *37*.
Xie, M., and Chagin, A.S. (2021). The epiphyseal secondary ossification center: Evolution, development and function. Bone *142*, 115701.
Xiong, Z.M., LaDana, C., Wu, D., and Cao, K. (2013). An inhibitory role of progerin in the gene induction network of adipocyte differentiation from iPS cells. Aging (Albany NY) *5*, 288-303.

Zannettino, A.C., Paton, S., Arthur, A., Khor, F., Itescu, S., Gimble, J.M., and Gronthos, S. (2008). Multipotential human adipose-derived stromal stem cells exhibit a perivascular phenotype in vitro and in vivo. J Cell Physiol *214*, 413-421.
Zhang, J., Lian, Q., Zhu, G., Zhou, F., Sui, L., Tan, C., Mutalif, R.A., Navasankari, R., Zhang, Y., Tse, H.F.*, et al.* (2011). A human iPSC model of Hutchinson Gilford Progeria reveals vascular smooth muscle and mesenchymal stem cell defects. Cell Stem Cell *8*, 31-45.
Zhang, Y., Parmigiani, G., and Johnson, W.E. (2020). ComBat-seq: batch effect adjustment for RNA-seq count data. NAR Genom Bioinform *2*, lqaa078.
Zhou, Y., Zhou, B., Pache, L., Chang, M., Khodabakhshi, A.H., Tanaseichuk, O., Benner, C., and Chanda, S.K. (2019). Metascape provides a biologist-oriented resource for the analysis of systems-level datasets. Nat Commun *10*, 1523.
Zoetis, T., Tassinari, M.S., Bagi, C., Walthall, K., and Hurtt, M.E. (2003). Species comparison of postnatal bone growth and development. Birth Defects Res B Dev Reprod Toxicol *68*, 86-110.

Figure Legends:

Figure 1
A) Summary table of processes related to DNA maintenance and epigenetics, represented as transcriptional up or downregulation based on RNA-seq of young/teenager progeria patient derived fibroblasts compared to age matched, middle age or old control patients.
B) Heat map of RNA-seq transcriptome analysis for 976 selected genes related to DNA maintenance and epigenetics. The heat map shows per-gene z-score computed from batch effect corrected log2 read count values, genes in rows and 29 patient samples (progeria and young/adult/old control) organized in columns. Genes were hierarchically clustered based on Euclidean distance and average linkage. Within each cohort, columns are organized by patient age.
C) Comparison of young progeria patients versus middle age or old donor control fibroblasts. Enriched ontology clusters for upregulated genes related DNA maintenance and epigenetics, as characterized by Metascape analysis.
D) Comparison of teen-aged progeria patient fibroblast versus old donor control fibroblasts. Enriched ontology clusters for up regulated genes related to DNA maintenance and epigenetics, as characterized by Metascape analysis.

Figure 2
A) Heat map of RNA-seq transcriptome analysis for 585 selected genes related to repair. Data presented as in Figure 1B.
B) Heat map of RNA-seq transcriptome analysis for 145 selected genes related to extra cellular matrix. Data presented as in Figure 1B.
C) Summary table of processes related to repair and extra cellular matrix organization, represented as up or downregulation in transcription based on RNA-seq of young/teenager progeria patient derived fibroblasts, compared to middle age or old control patients.

Figure 3
A) Summary table of processes related to bone and cartilage development and homeostasis represented as up or downregulated transcription based on RNA-seq of young progeria patient derived fibroblasts compared to age matched, middle age or old control patients.
B) Heat map of RNA-seq transcriptome analysis for 165 selected genes related to bone and cartilage development. Data presented as in Figure 1B.

C) Comparison of young progeria patients versus old donor control fibroblasts. Enriched ontology clusters for upregulated genes related bone and cartilage development and homeostasis, as characterized by Metascape analysis.
D) Comparison of young progeria patients versus old donor control fibroblasts. Enriched ontology clusters for downregulated genes related to cation homeostasis, as characterized by Metascape analysis.
E) Comparison of young progeria patients versus middle age control fibroblasts. Enriched ontology clusters for downregulated genes related to bone development and homeostasis, as characterized by Metascape analysis.

Figure 4
A) Summary table of processes related to fat cell differentiation and lipid metabolism, represented as up or downregulation in transcription based on RNA-seq of young/teenager progeria patient derived fibroblasts, compared to age matched, middle age or old control patients.
B) Heat map of RNA-seq transcriptome analysis for 134 selected genes related to fat cell differentiation and lipid metabolism. Data presented as in Figure 1B.
C) Comparison of young progeria patients versus middle age or old donor control fibroblasts. Enriched ontology clusters for upregulated genes related to fat and lipid metabolism, as characterized by Metascape analysis.

Figure 5
A) Summary table of processes related to blood vessel homeostasis, represented as up or downregulation in transcription based on RNA-seq of young/teenager progeria patient derived fibroblasts, compared to age matched, middle age or old control patients.
B) Heat map of RNA-seq transcriptome analysis for 131 selected genes related to blood vessel homeostasis. Data presented as in Figure 1B.
C) Comparison of young progeria patients versus middle-aged donor control fibroblasts. Enriched ontology clusters for upregulated genes related to blood vessel development, as characterized by Metascape analysis.
D) Comparison of teen-aged progeria patient fibroblast versus age-matched control fibroblasts. Enriched ontology clusters for up regulated genes related to blood vessel development, as characterized by Metascape analysis.

Figure 6
A) Summary table of processes related to muscle and cardiac muscle development, represented as up or downregulation in transcription based on RNA-seq of young/teenager progeria patient derived fibroblasts, compared to middle age or old control patients.
B) Heat map of RNA-seq transcriptome analysis for 261 selected genes related to muscle development. Data presented as in Figure 1B.
C) Comparison of young progeria patients versus middle-aged and old donor control fibroblasts and of teen-aged progeria patients versus old donor controls. Enriched ontology clusters for upregulated genes related to muscle development, as characterized by Metascape analysis.

Figure 7
A) Heat map of RNA-seq transcriptome analysis for 25 selected genes related to endochondral ossification. The heat map shows per-gene z-score computed from batch effect corrected log2 read count values, genes in rows and 29 patient samples (progeria and young/adult/old control) organized in columns. Genes were hierarchically clustered based on Euclidean distance and average linkage. Blue lines separate young infants (0-3 y/o) from children (4-7 y/o) and older children (7-10 y/o). Genes related to WNT5a biology highlighted (red circle)
B) Abridged signaling pathway for WNT5a, highlighting the roles of the genes whose transcription is affected in young HGPS patients compared to their aged-matched controls.

Figure 8. Changes in chromatin architecture in HGPS cells: translocations, compartment strength and identity, and correlation to genes of interest.
A) 2.5-Mb Hi-C heatmaps for AG03257-P7 (Mother, WT), and HGPS patients (HGADFN167-P19 and AG11513-P7) Translocations between chromosomes appear as high interaction frequency regions (red) away from the diagonal. A translocation between chromosomes 3 and 11 is apparent in AG11513 cells (circle).
B) Log ratio of 2.5 Mb contact frequency in Progeria (167-P19) vs. healthy father (168-P16). Loss of telomere interactions is notable as blue patches in the corner of each chromosome. C) TAD boundary strength boxplots calculated using the InsulationScore approach between early (left) and late (right) passage Progeria cells minus their respective controls. Boxes represent the upper and lower quartiles with the center line as the median. Upper whiskers extend 1.5×IQR beyond the upper quartile, and lower whiskers extend either 1.5×IQR below the lower quartile or to the end of the dataset. D) Plots of the first eigenvector for a section of chromosome 12, obtained from principal component analysis (PC1) of 250-kb binned Hi-C data for control fibroblasts (Mother AG03257, Father HGADFN168) and HGPS fibroblasts (HGADFN167 and AG11513). Compartment identity remains predominantly unchanged (A compartment: Red, B compartment: Blue). E) Graphs showing the A-A compartment interaction strength (red) and B-B compartment interaction strength (blue) within each chromosome for related father and child cell lines (HGADFN168, HGADFN167). Samples were collected a both early (left; P12) and late passages (middle; P19 for Progeria and P27 for father). Comparison between the two samples (right) shows that the HPGS cell line shows a marked decrease in A-A compartment interaction strength in late passages in the majority of chromosomes. F) Eigen 1 values represent the compartment identity (same as plotted in D) for genes identified in this study as upregulated (left) or downregulated (right) in the 0–7-year-old age matched comparison. While differences between groups are not significant overall (Kruskal-Wallis), a subset of downregulated genes appear to be changing conformation to a B compartment in progeria samples (box). Violin plots for the global distribution of values; median denoted by thick dashed line, 25th and 75th percentiles highlighted as thin dashed lines. Percentages of genes in the B compartment indicated in box below downregulated gene graph. G) Compartment identity for genes identified in this study as upregulated (left) or downregulated (right) in the 0–7-year-old HGPS samples compared to normal middle-aged controls.
H) Compartment identity for genes identified in this study as upregulated (left) or downregulated (right) in the 0–7-year-old HGPS samples compared to old-aged controls.

Figure 9
40-kb resolution heatmaps for the parental and HGPS cell lines, around the WNT5a gene (highlight: blue), aligned to their associated compartment and LAD tracks. The gene localizes at the boundary of a switch to the B compartment in HGPS cells

Figure 10
Discussion model. HGPS affects differentiation commitment and subsequent biology of priority during early development, which results in premature depletion of MSC pools.

Movie 1: A visual explanation of ideas presented in the Discussion, hypotheses derived from transcriptomics results.

Supplementary Figures and Tables

Supplementary Figure 1. Batch clustering correction.
A) Principal component analysis (PCA) of the datasets used in this study before batch correction. Samples segregate primarily by lab of origin (red circles). Solid color markers: Progeria, hollow markers: normal controls, triangles: female, circles: male.

B) PCA after batch correction. Samples primarily segregate by progeria/control phenotype. Dotted line denotes an arbitrary margin between cohorts. Solid color markers: Progeria, hollow markers: normal controls, triangles: female, circles: male. Purple circles denote patients that are mismatched from the rest of their respective groups.

Supplementary figure 2. Genes of interest vs LADS

A) The genomic regions for downregulated genes identified in our age comparisons were compiled with the LAD identity found in a father-HGPS child fibroblasts (HGADFN168 and HGADFN167, respectively). Comparisons are presented as follows, from left to right: Young HGPS (0-7 years old) compared to middle-aged controls, young HGPS patients compared to old controls, teenaged HGPS compared to middle-aged controls and teenaged HGPS compared to old controls. Differences between al groups are significant (Kruskal-Wallis $p<0.001$) Violin plots for the global distribution of values; median denoted by thick dashed line, 25th and 75th percentiles highlighted as thin dashed lines

B) The genomic regions for up regulated genes identified in our age comparisons were compiled with the LAD identity found in a father-HGPS child fibroblasts (HGADFN168 and HGADFN167, respectively). Comparisons are presented as follows, from left to right: Young HGPS (0-7 years old) compared to middle-aged controls, young HGPS patients compared to old controls, teenaged HGPS compared to middle-aged controls and teenaged HGPS compared to old controls. Differences between al groups are significant (Kruskal-Wallis $p<0.001$) Violin plots for the global distribution of values; median denoted by thick dashed line, 25th and 75th percentiles highlighted as thin dashed lines

C) LAD distribution along chromosome 1 and 21. LAD identity remains consistent among samples, with small regional changes in LAD definition in specific areas (highlighted- rectangle). The greatest difference among samples is the strength in LAD definition, as characterized by smaller positive and negative values

D) The genome-wide distribution of LADs, as characterized by DamID-seq shows that normal fibroblast lines HGADFN168 (belonging to a father of an HGPS patient) and HFFc6 (human foreskin fibroblast), show a characteristic bimodal distribution in LAD intensity around positive (LAD) and negative (non-LAD) values. In contrast, LAD values for the HGPS cell line HGADFN168 distribute normally, around zero.

Supplementary Figure 3

40-kb resolution heatmaps for the parental and HGPS cell lines, around the PTHLH gene (highlight: blue), aligned to their associated compartment and LAD tracks. The gene localizes to the A compartment in both HGPS and control cell lines. A called LAD domain is present in HGPS cells.

Supplementary Table 1. RNA-seq datasets from progeria patients used in this study
Supplementary Table 2. RNA-seq datasets from adult controls used in this study
Supplementary Table 3. RNA-seq datasets from children controls used in this study
Supplementary Table 4. Hi-C Data Statistics

A

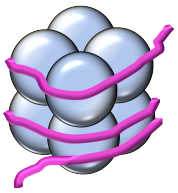

Patient	Young			Teen		
Comparison	Age Matched	Middle age	Old	Age Matched	Middle age	Old
UP						
Down						

- Epigenetic regulation of gene Silencing
- Negative regulation of gene expression, epigenetic
- Chromatin silencing
- Senescence associated heterochromatin
- Chromatin organization involved in negative reg. transcription
- DNA repair
- Response to UV
- Double strand DNA repair
- Cellular response to DNA damage stimulus
- DNA Recombination
- Regulation of gene silencing
- Histone Methylation
- Histone Modification
- Chromatin modifying enzymes

B

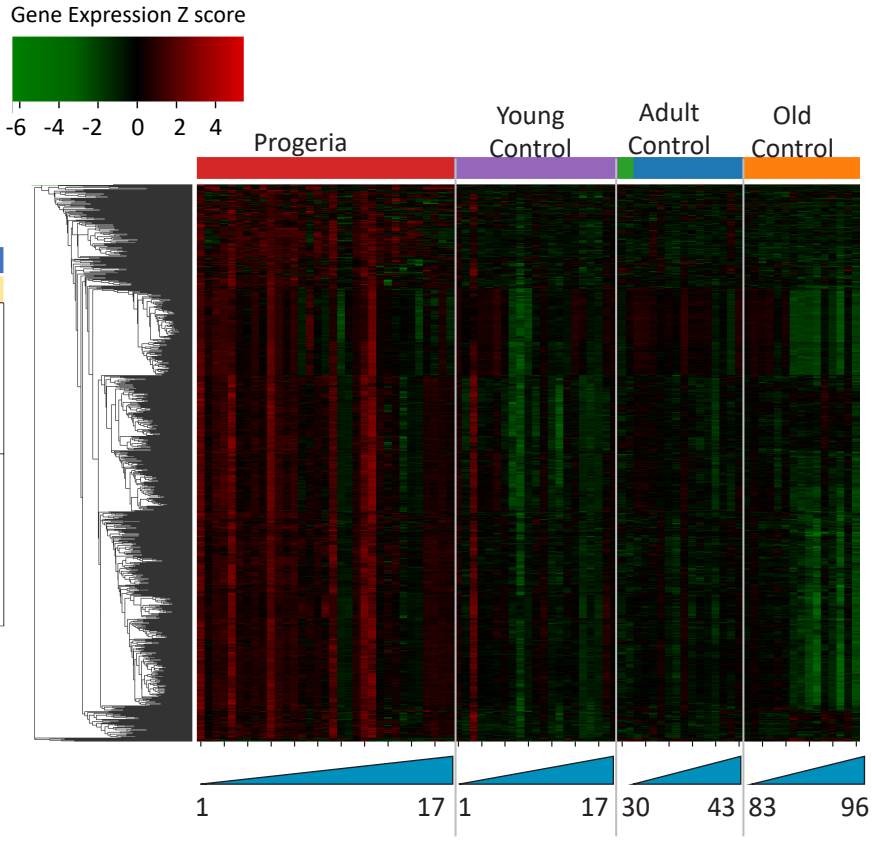

C

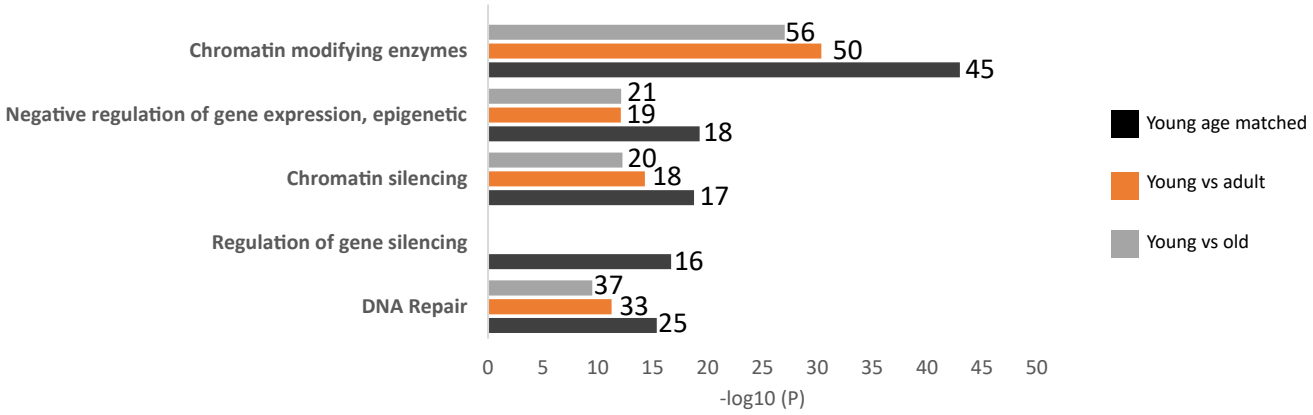

D

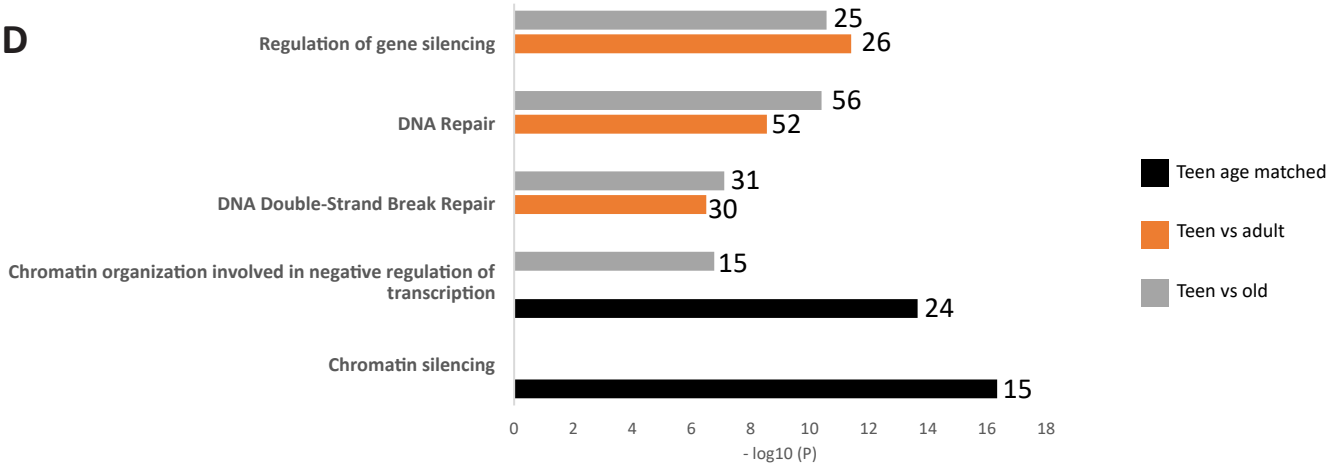

Figure 1

A

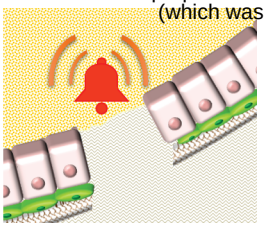

Tissue Repair

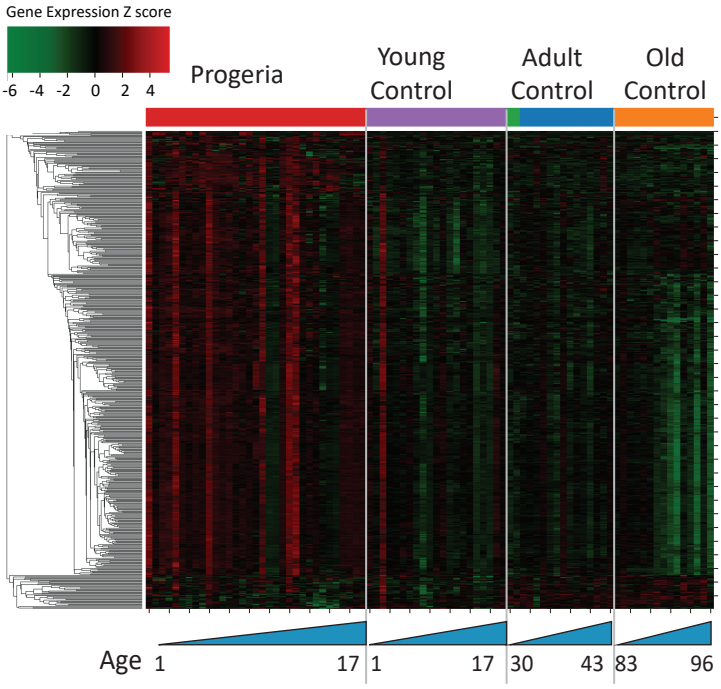

B

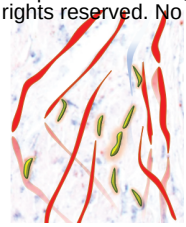

Extracellular matrix

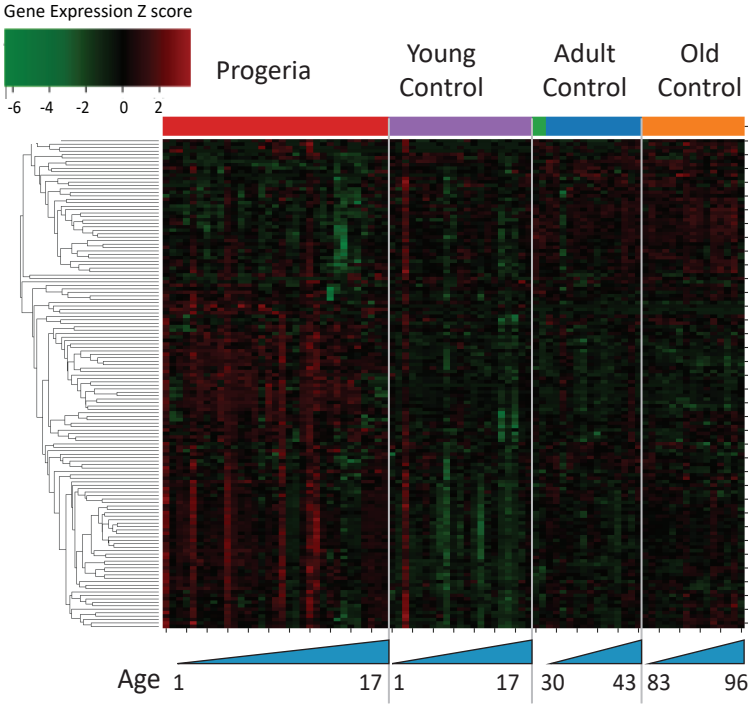

C

Patient	Young		Teen	
Comparison	Middle age	Old	Middle age	Old
Up	● ■	● ■	● ■	★
Down	● ●	● ● ●		

- Extracellular matrix organization
- Extracellular matrix disassembly
- Negative regulation of TGFβ response
- BMP signaling
- Blood coagulation
- Response to wound healing
- Collagen Organization
- Collagen catabolic process
- Platelet activation
- Response to mechanical stimulus
- ★ Effect of Progerin on genes involved in Hutchinson-Gilford Progeria

Figure 2

A

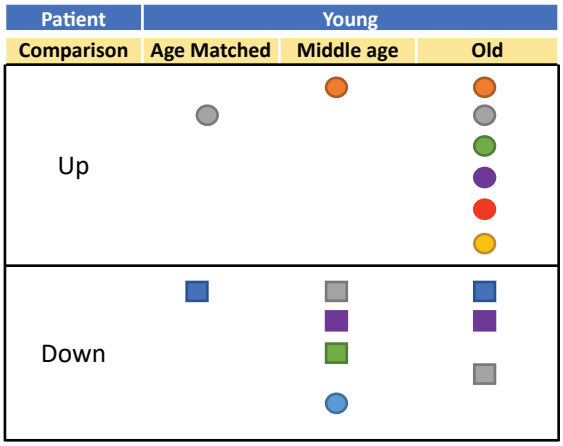

- Osteoblast differentiation
- Mesenchymal cell development
- Skeletal development
- Regulation of chondrocyte differentiation
- Connective tissue development
- Cartilage development
- Trabeculae morphogenesis
- Positive regulation of cytosolic calcium concentration
- Ion Concentration
- Calcium homeostasis
- Cytosolic calcium transport
- Cation homeostasis

B

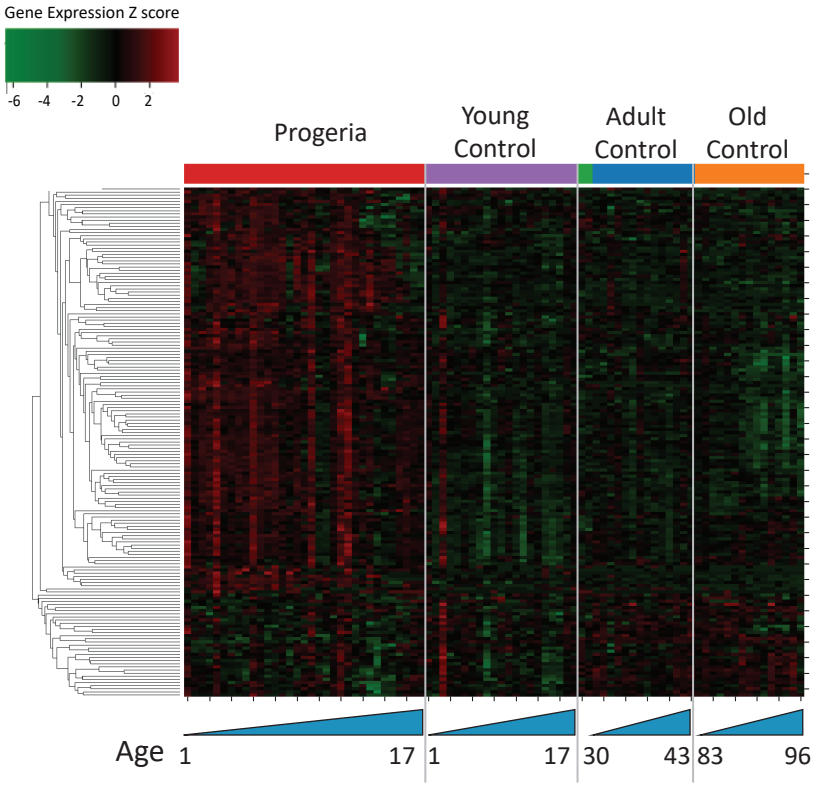

C

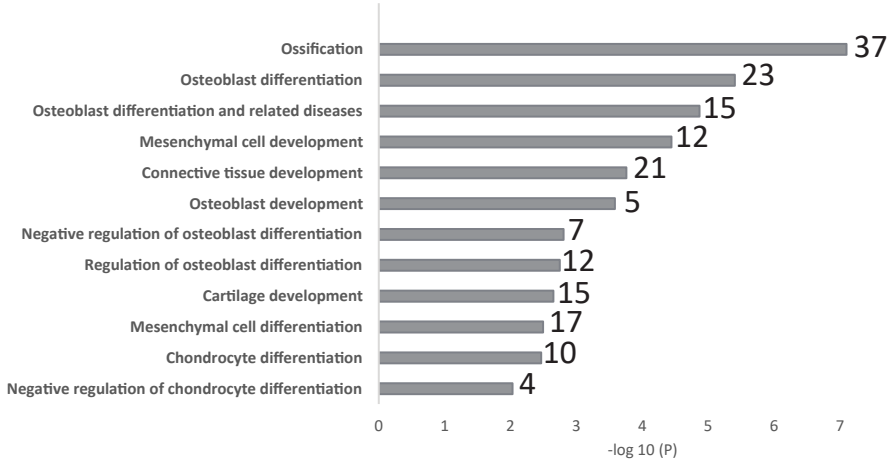

D

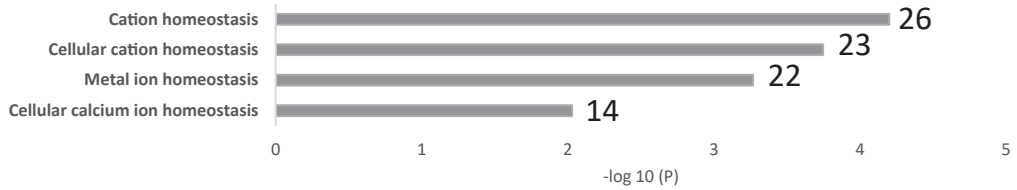

E

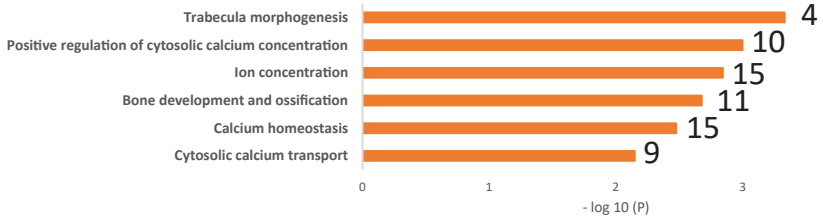

Figure 3

A

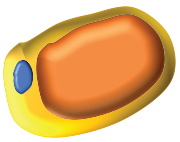

Patient	Young			Teen
Comparison	Age Matched	Middle age	Old	Age Matched
Up				● ■
Down	●	● ● ●	● ● ● ■ ■ ■ ■	

- Fat cell differentiation
- Cellular response to ketones
- Cellular response to lipid
- Cellular response to steroids
- Lipid organization
- Lipid biosynthetic process
- Lipid transport
- Metabolism of lipids
- Lipid localization
- Regulation of lipid storage

B

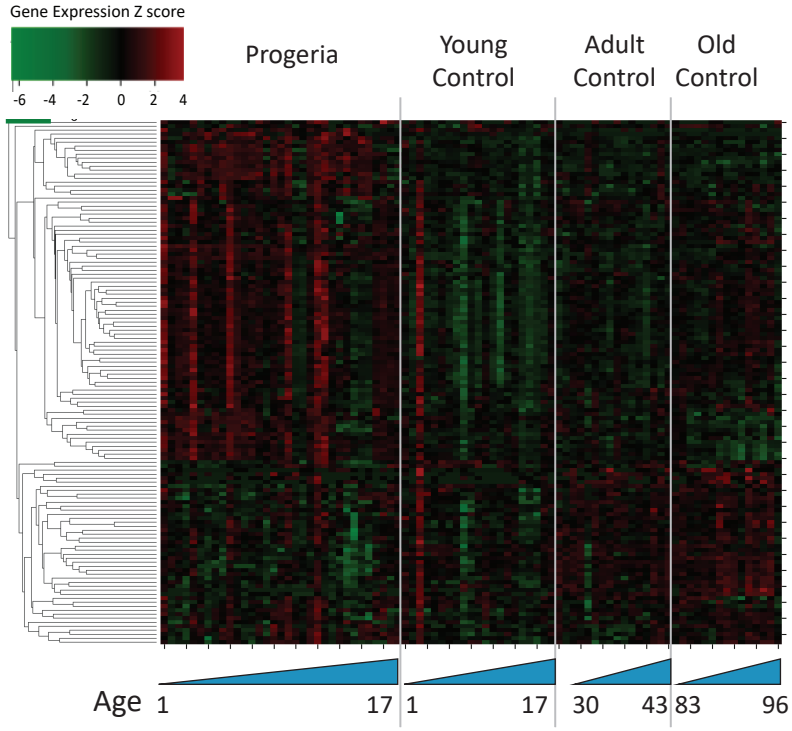

C

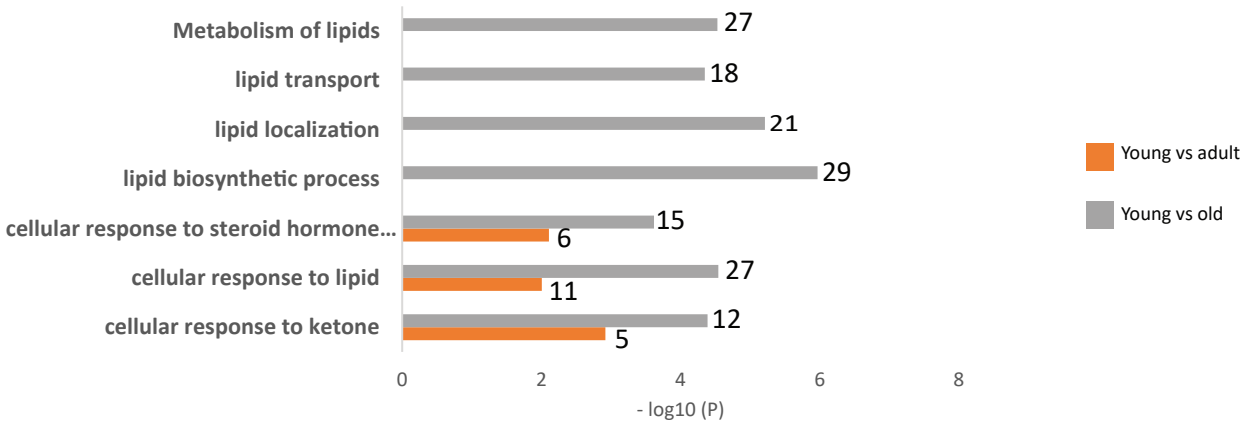

Figure 4

A

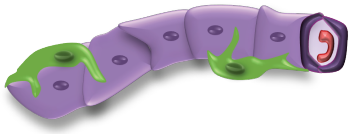

Patient	Young		Teen
Comparison	Age Matched	Old	Age Matched
Up	●	● ● ●	● ● ●
Down		●	

- Blood vessel morphogenesis
- Angiogenesis
- Blood vessel development
- Blood vessel maturation
- Regulation of vascular development

B

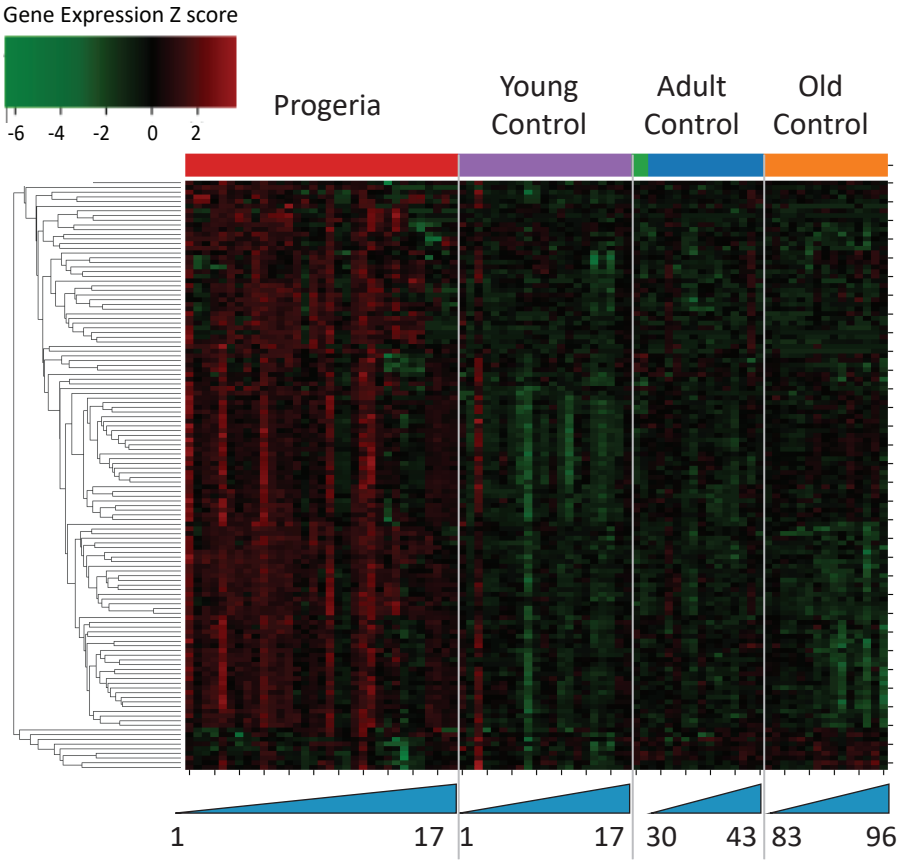

C

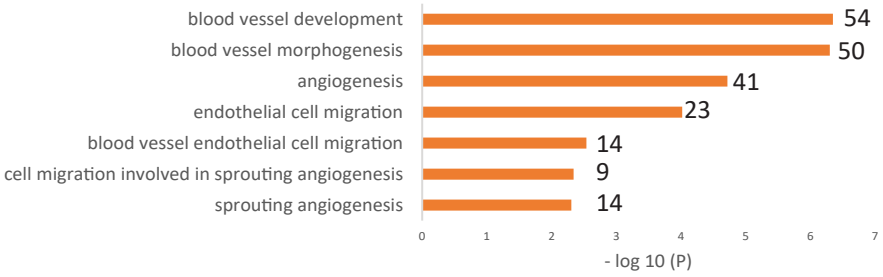

D

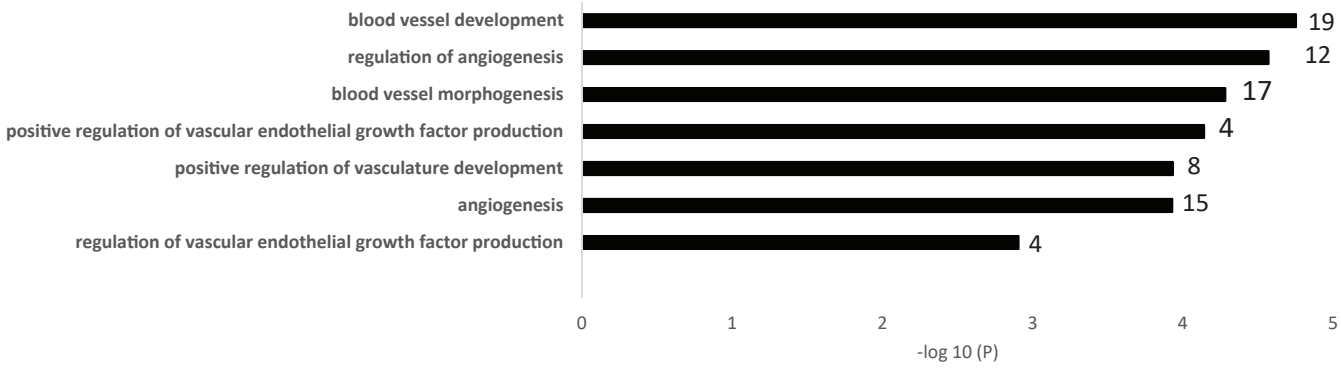

Figure 5

A

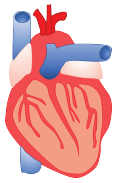

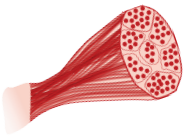

Patient	Young		Teen
Comparison	Middle age	Old	Old
Up			

Cardiocyte differentiation
Cardiac muscle differentiation
Cardiac muscle tissue development
Heart development
Striated Muscle differentiation
Muscle Tissue development
Muscle structure development
Muscle organ development

B

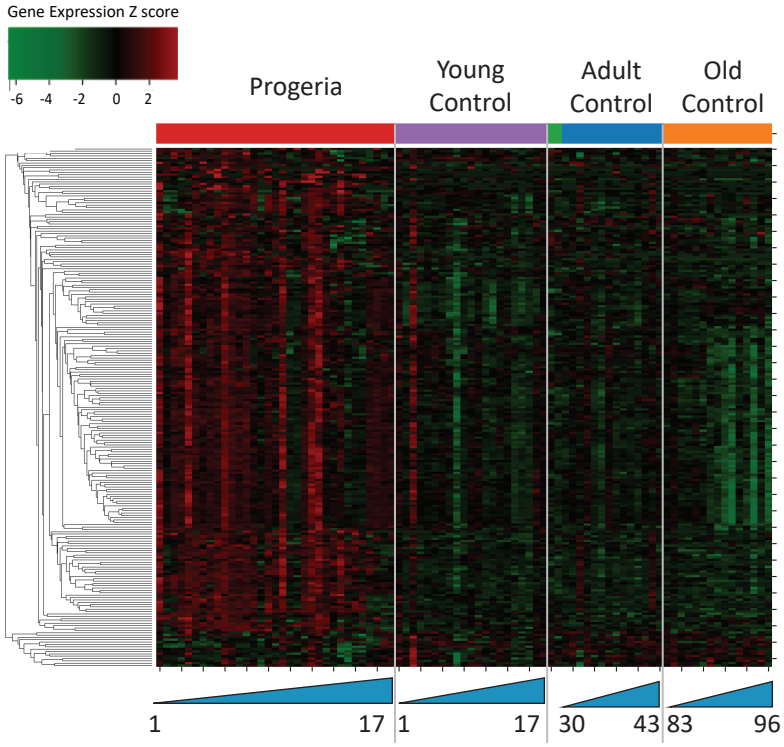

C

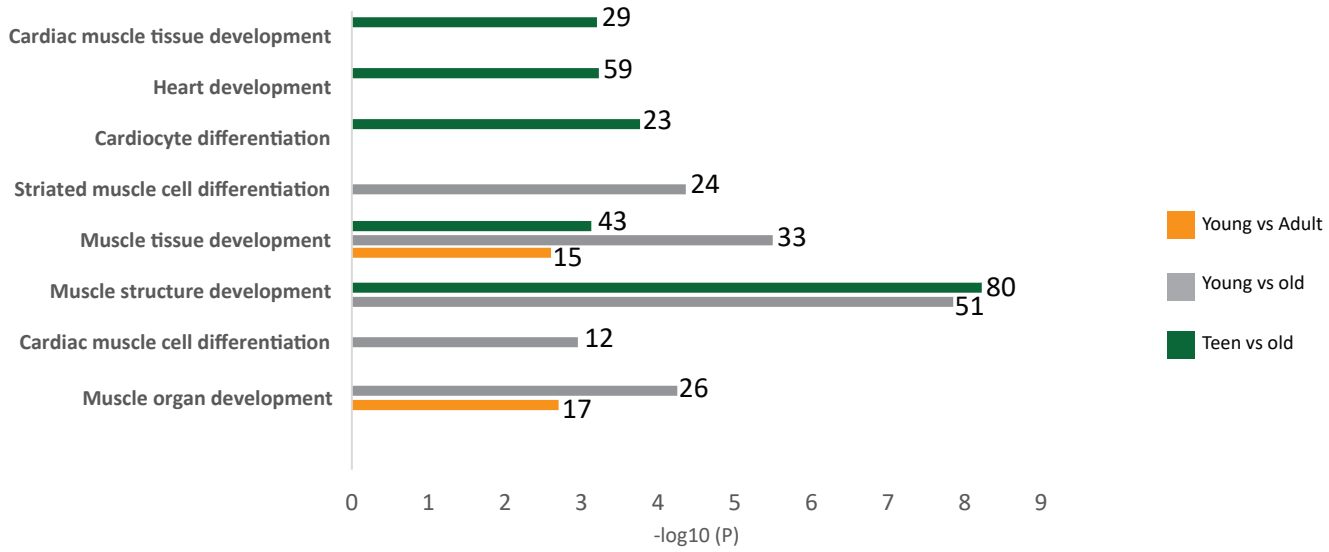

Figure 6

A

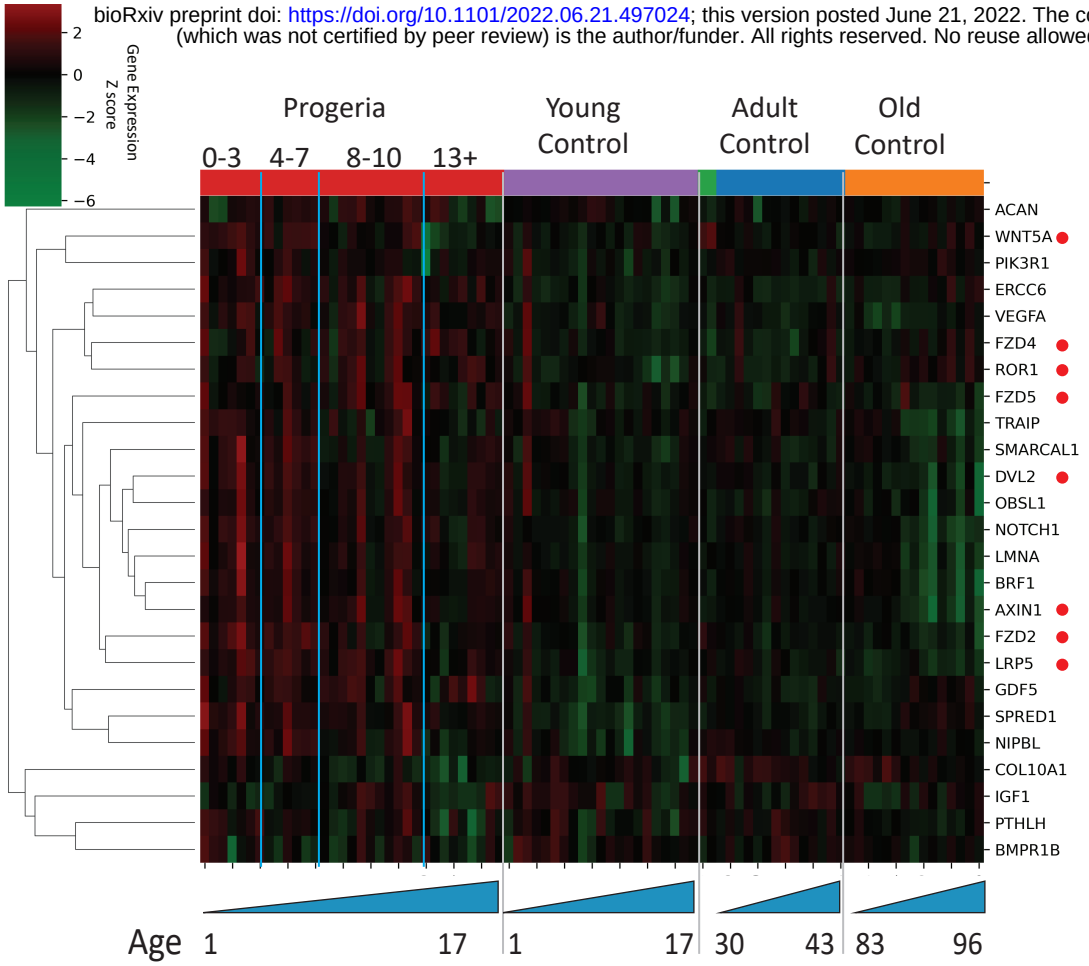

B

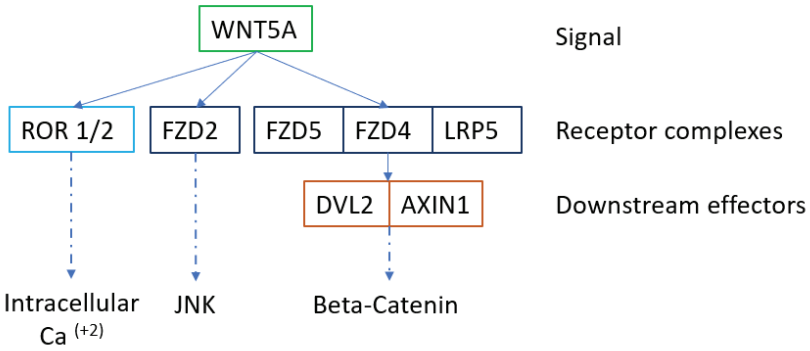

Figure 7

Figure 8

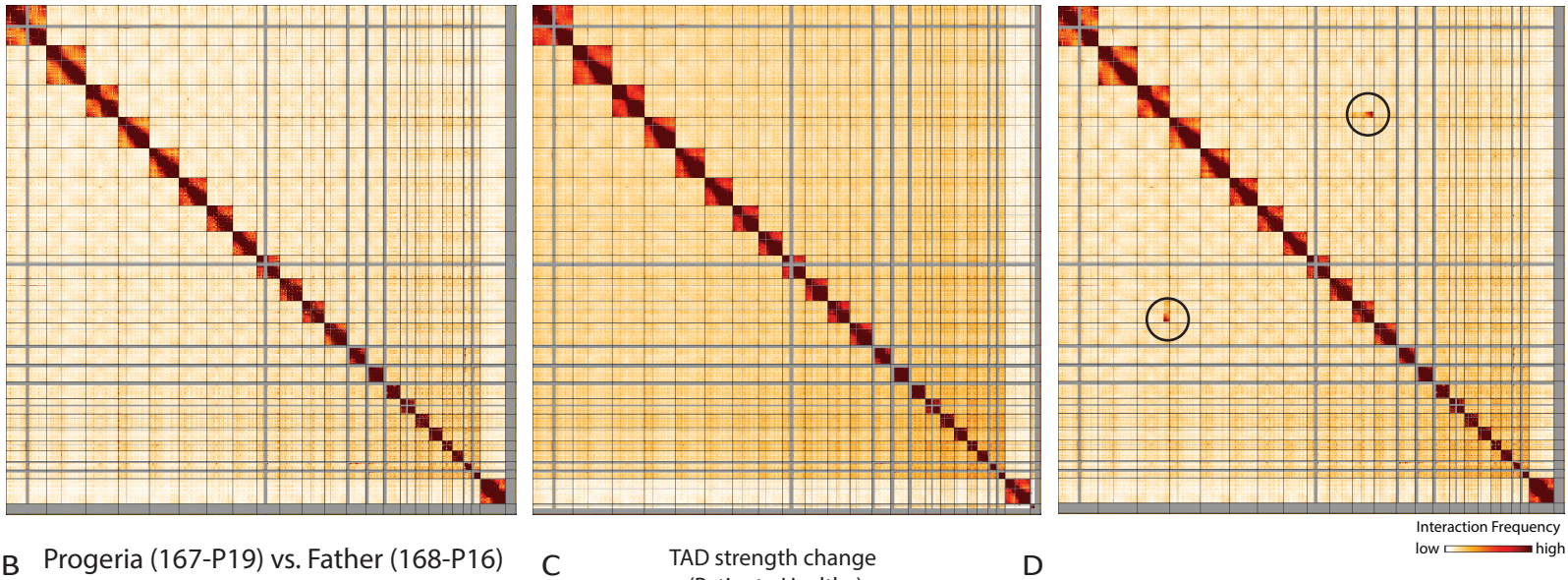

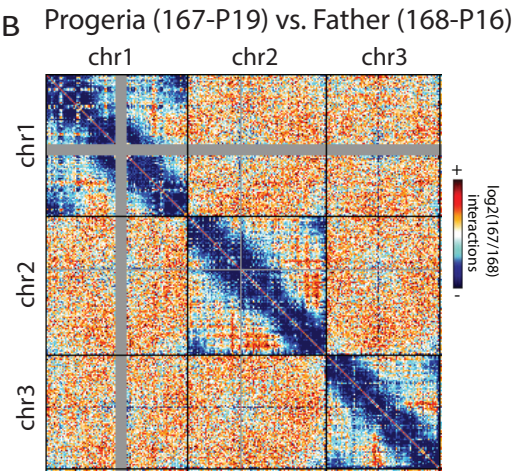

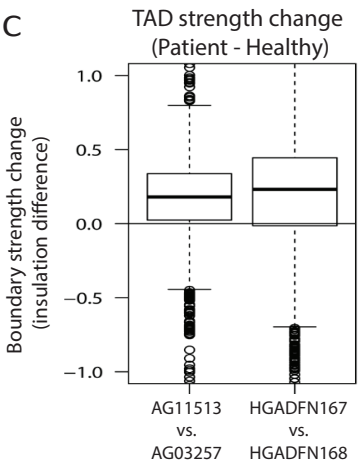

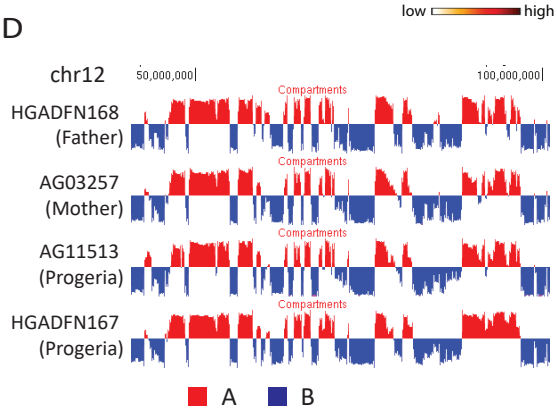

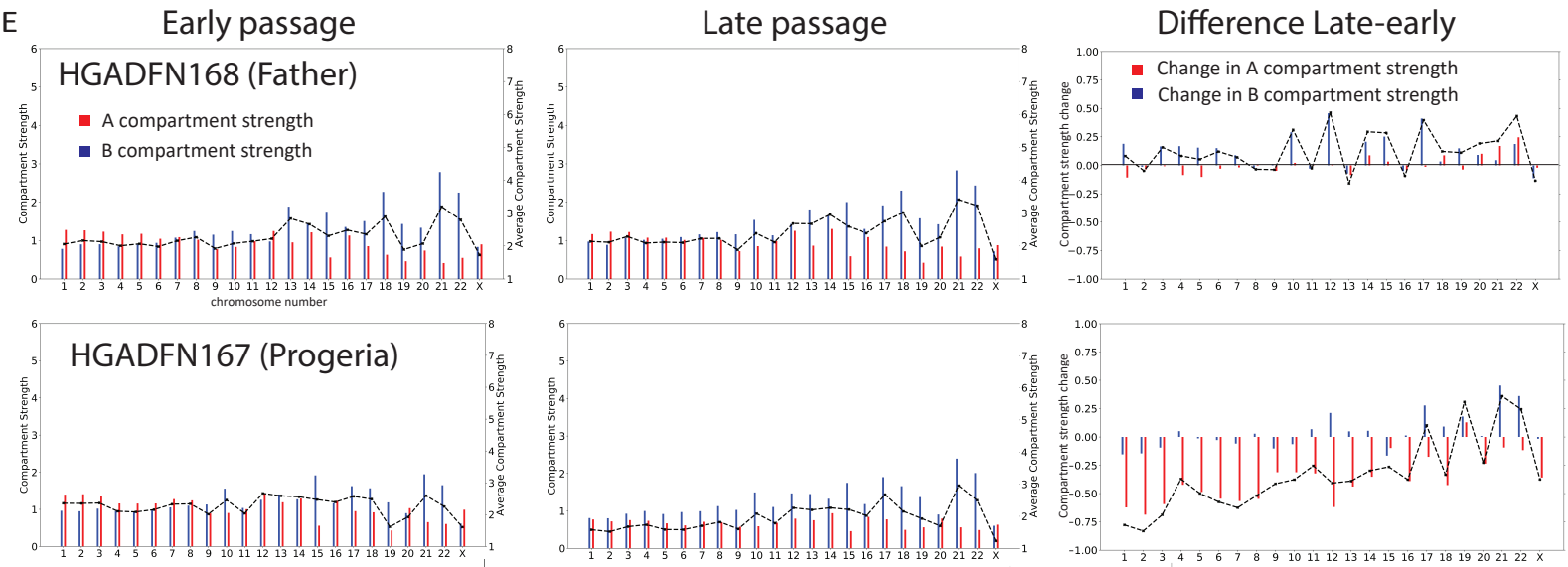

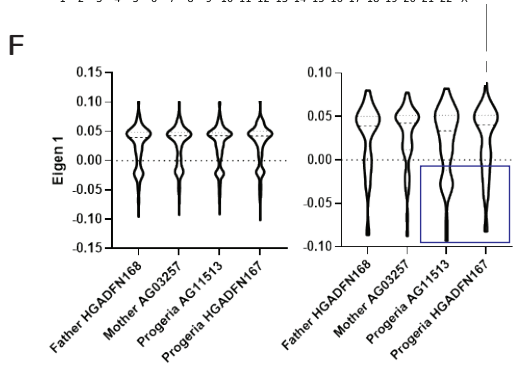

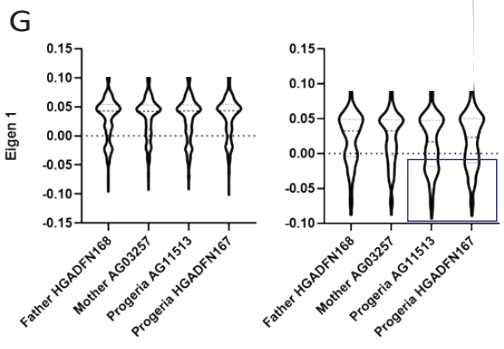

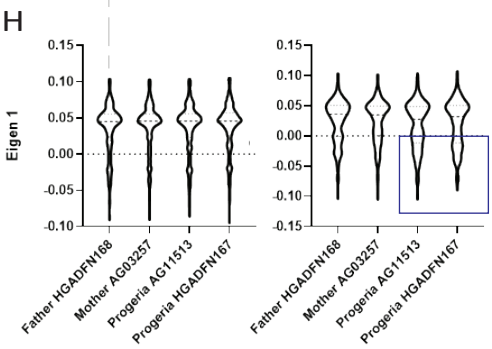

Percent bins in the B compartment:				
	20.4	16.3	24.4	26.5
	29.4	25.8	38.0	35.0
	26.7	24.4	34.0	30.7

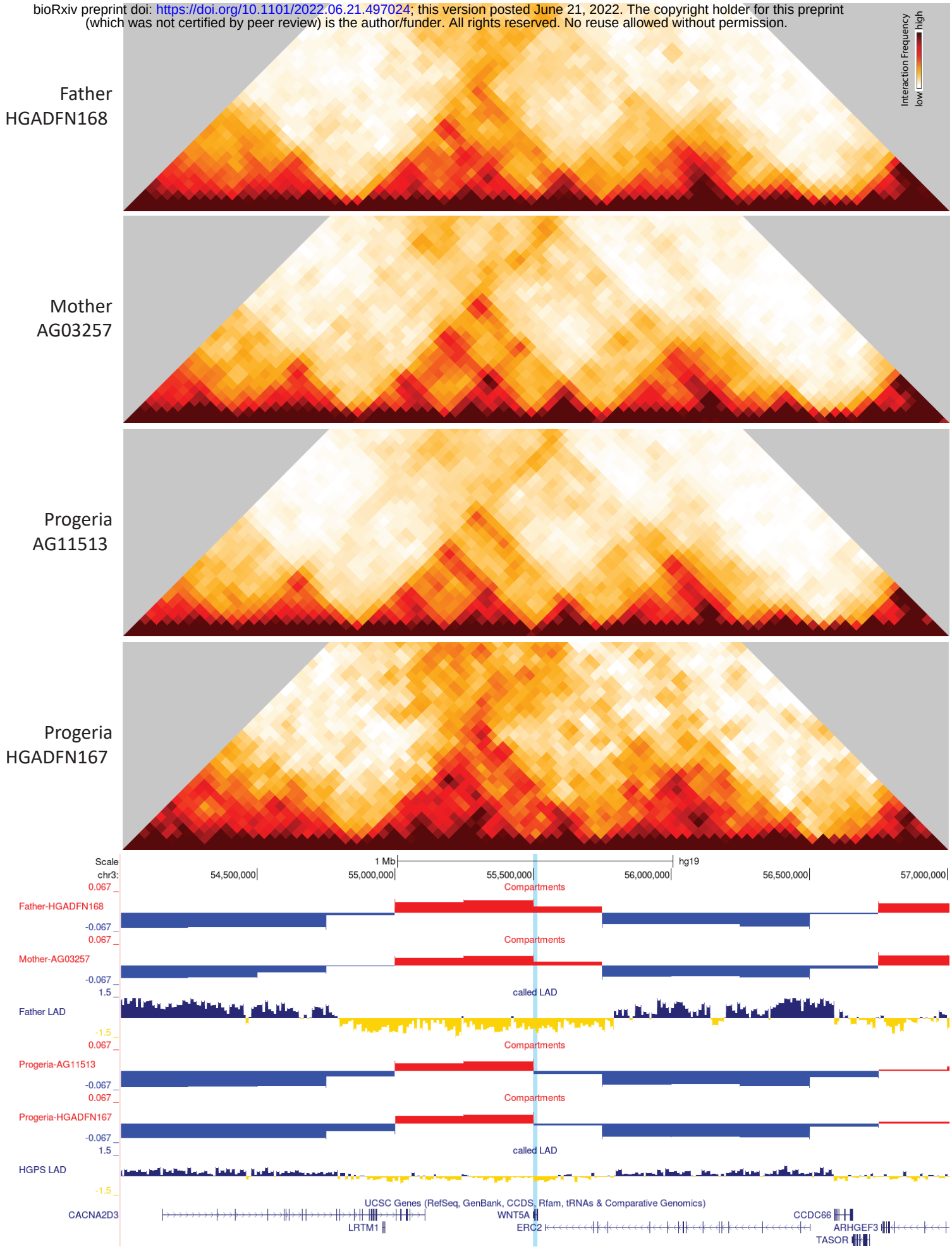

Figure 9

A

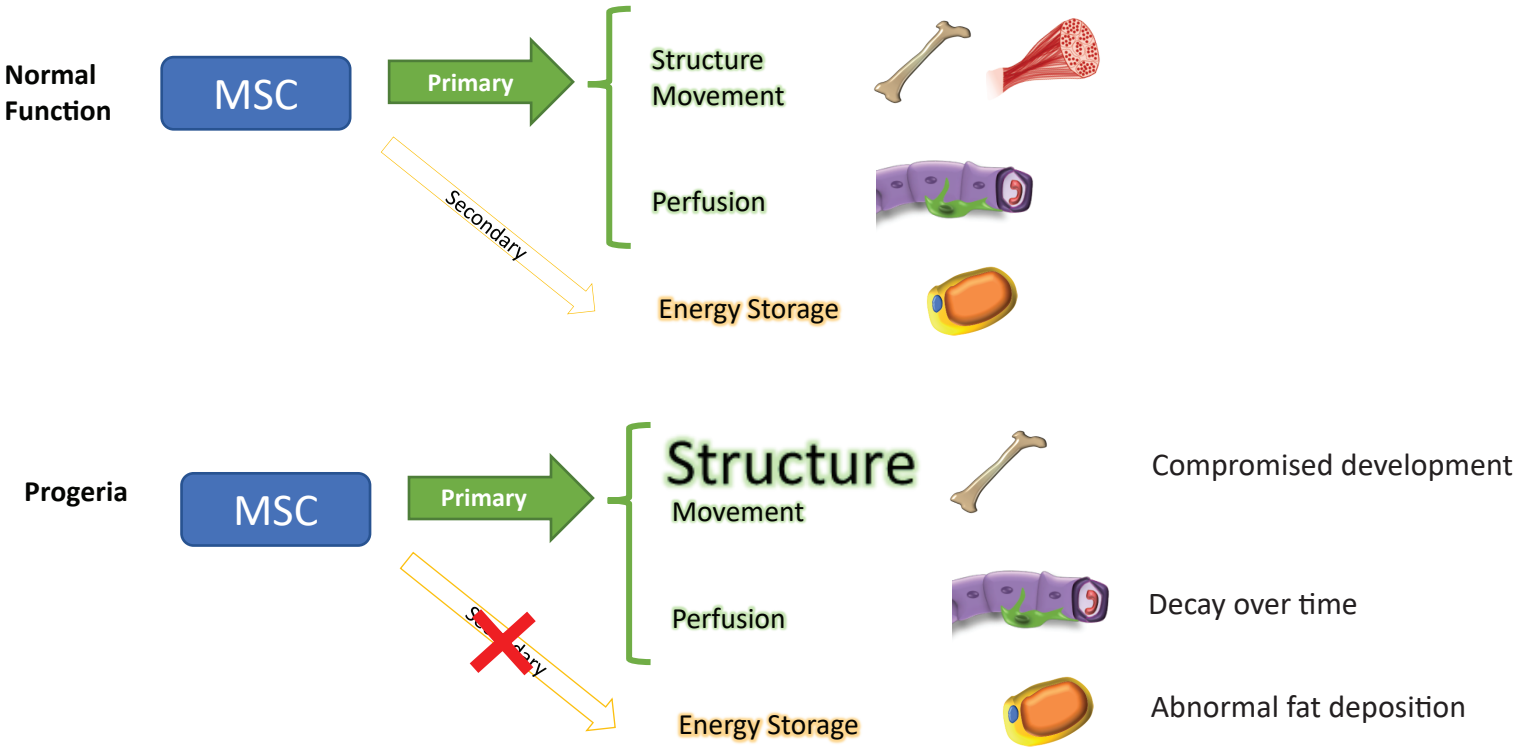

B

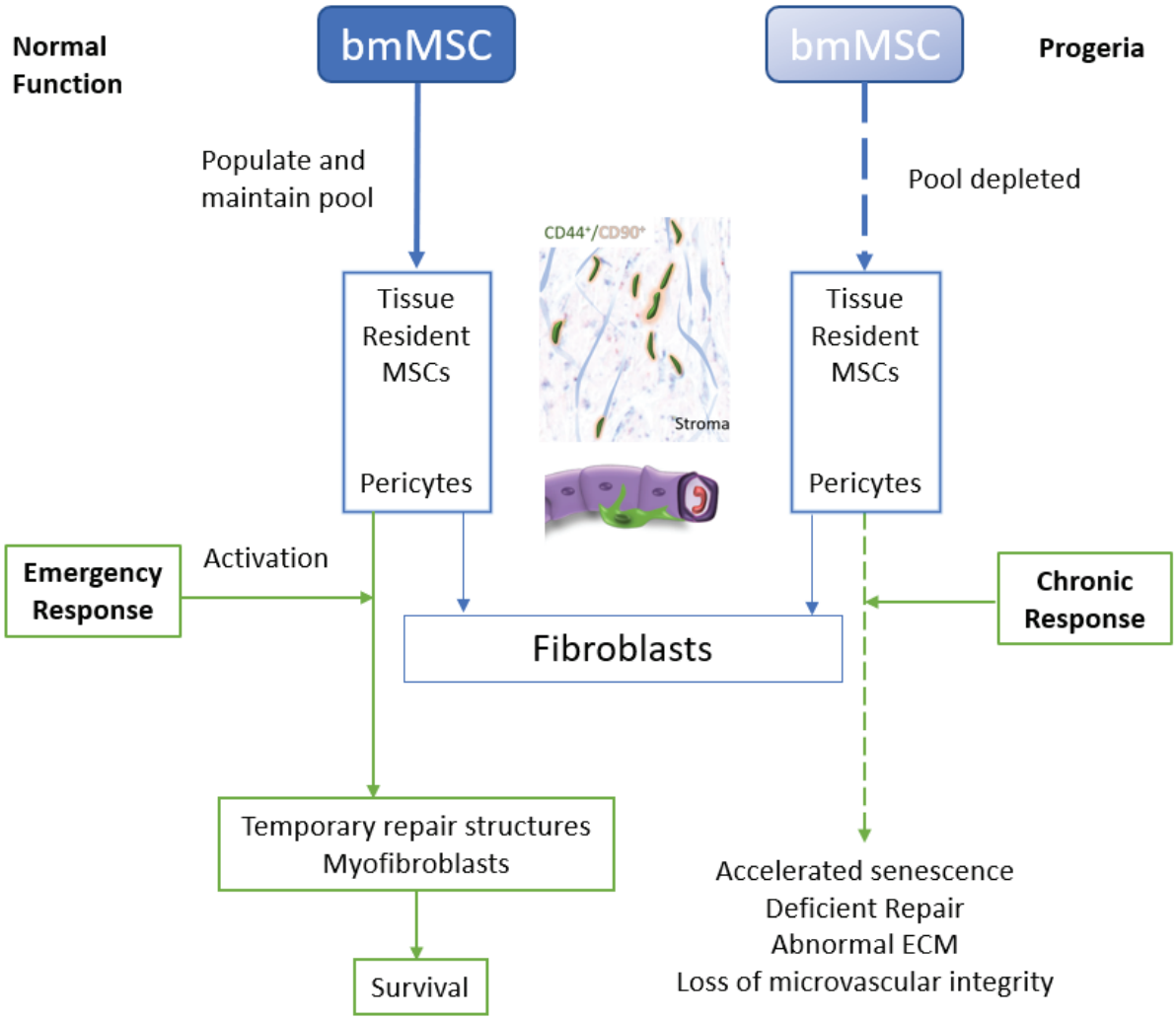

Figure 10